

**MOLECULAR CLONING, EXPRESSION, AND
CHARACTERIZATION OF GLUTATHIONE-S-
TRANSFERASE AS A NOVEL TARGET IN ANTI-
MALARIAL DRUG DESIGN AND DISCOVERY**

By

**MOHAMMED NOORALDEEN MAHMOD
AL-QATTAN**

**Thesis submitted in fulfillment of the requirements for the degree of
Doctor of Philosophy in Science**

March 2015

ACKNOWLEDGEMENT

To all Muslim brothers:

"Allah will deprive usury of all blessing, but will give increase for deeds of charity" (Quran 2: 276). In a hadith narrated by Abu 'Amir or Abu Malik Al-Ash'ari: that he heard the Prophet saying, "From among my followers there will be some people who will consider illegal sexual intercourse, the wearing of silk, the drinking of alcoholic drinks and the use of musical instruments, as lawful. And there will be some people who will stay near the side of a mountain and in the evening their shepherd will come to them with their sheep and ask them for something, but they will say to him, 'Return to us tomorrow.' Allah will destroy them during the night and will let the mountain fall on them, and He will transform the rest of them into monkeys and pigs and they will remain so till the Day of Resurrection." (No. 5226, Sahih Al-bukhari).

Allah's wisdom ruled that sins do not provide richness and development even if sin-fullers pretend to have it. Furthermore, pretending to have what you have not is a sin. It is related from Asma' from the Prophet (may Allah bless him and grant him peace) that a woman said, "Messenger of Allah, I have a co-wife. Would it be a sin if I were to pretend to have received something from my husband which he has not given me?" The Prophet said, "Anyone who pretends to have received something he has not been given is like someone who wears two spurious garments [i.e. someone who dresses up to give a false impression]." (No.4921, Sahih Al-bukhari)

Attending the path of disbelievers seeking for development and reputation is an attribute of Monafiqin and soon they will blame themselves when ALLAH give victory to believers. {O you who have believed, do not take the Jews and the Christians as allies. They are [in fact] allies of one another. And whoever is an ally to them among

you - then indeed, he is [one] of them. Indeed, Allah guides not the wrongdoing people (51) So you see those in whose hearts is disease hastening into [association with] them, saying, "We are afraid a misfortune may strike us." But perhaps Allah will bring conquest or a decision from Him, and they will become, over what they have been concealing within themselves, regretful (52)} (Ayah 51-52, Surah Al-Maidah).

The beneficial knowledge is really that which descended from ALLAH regarding His names, actions and attributes. {So turn away from whoever turns his back on Our message and desires not except the worldly life (29) That is their sum of knowledge. Indeed, your Lord is most knowing of who strays from His way, and He is most knowing of who is guided (30)} (Surah Al-Najm ayah 29-30)

Other knowledge even beyond quantum level is merely superficial and will not prevent punishment if it comes. {Have they not traveled through the land and observed how was the end of those before them? They were more numerous than themselves and greater in strength and in impression on the land, but they were not availed by what they used to earn (82) And when their messengers came to them with clear proofs, they [merely] rejoiced in what they had of knowledge, but they were enveloped by what they used to ridicule (83) And when they saw Our punishment, they said," We believe in Allah alone and disbelieve in that which we used to associate with Him." (84) But never did their faith benefit them once they saw Our punishment. [It is] the established way of Allah which has preceded among His servants. And the disbelievers thereupon lost [all] (85)} (Ayah 82-85, Sura Ghafir).

The prophet Mohammed (PBUH) said "Does not thank Allah the person who does not thank the people" (No. 211, Al-adab Al-mofrad for Bukhary). Therefore, I would like to thank each of Prof Madya Mohd Nizam Mordi (main supervisor), Prof. Sharif Mahsofi Mansor (co-supervisor and the director) and Prof Madya Dr. B.

Vicknasingam (kind supporter) at Centre For Drug Research, USM. Thanks and appreciations to Prof. Mohd Razip Samian (co-supervisor, keen teacher and grand brother), Prof. Mohd Nazalan Mohd Najimudin and Prof. Madya Shaida Fariza Sulaiman from School of biological sciences, USM as well as Dr. Teh Aik Hong from Centre for Chemical biology, USM. And also not forget to appreciate the efforts of the staff of Centre for Drug Research especially Mr. Rahim. I would like to thank my lab mates in 414 lab at school of biology; Faisal and Adrian Check for kind support and assistance. I would like to thank Universiti Sains Malaysia (USM) for supporting my study under the bountiful USM fellowship scheme. Thanks to my father, my stepmother and my wife for the kind assistance and wishes for my children (Zubaidah, Musa, Shuaib, Rufaida and Maryiah) to be from the Salheen (well-doers).

TABLE OF CONTENTS

	Page
ACKNOWLEDGEMENT	II
TABLE OF CONTENTS.....	V
LIST OF TABLES	XIII
LIST OF FIGURES	XVI
LIST OF SYMBOLS	XXXI
LIST OF ABBREVIATIONS	XXXII
ABSTRAK	XXXIV
ABSTRACT.....	XXXVI
CHAPTER 1 - INTRODUCTION.....	1
1.1 Problem statement.....	1
1.2 Malaria and anti-malarial compounds.....	4
1.3 Glutathione-s-transferases (GSTs).....	11
1.4 Classification of GSTs	12
1.5 General structure of cytosolic GSTs	13
1.6 General mechanisms for catalyzing chemical reactions employed by enzymes and GSTs.....	16
1.7 GSTs functions and substrates	19
1.7.1 Conjugation activity	19
1.7.2 Peroxidase activity	20
1.7.3 Isomerization activity.....	20
1.7.4 Toxicity potentiation activity	21
1.7.5 Ligand-in activity	21

1.7.6	Protein-interaction activity	22
1.8	GSTs in current study: leading aspects	25
1.8.1	Plasmodium falciparum GST (PfGST)	25
1.8.2	Human GST Pi-1 isoform (hGSTP1)	28
1.8.3	Mouse GST Mu-1 isoform (mGSTM1)	31
1.9	Cooperativity between subunits in GSTs	33
1.10	Classes of available GSTs inhibitors	34
1.11	Enzyme kinetics	42
1.11.1	Measurement of initial enzyme velocity	42
1.11.2	Modes of substrate binding in multiple substrate enzymes	43
1.11.3	Modes of reversible enzyme inhibition	47
1.11.4	Mode of interaction between two reversible enzyme inhibitors (double inhibition)	50
1.12	Drug design	50
1.12.1	Molecular optimization progresses by iterative exchange between searching algorithm and scoring function	51
1.12.2	Molecular representations during optimization	52
1.12.3	Application of <i>de novo</i> molecular design	53
1.13	X-ray crystallography	53
1.13.1	Protein X-ray crystallography	53
1.13.1.1	Protein crystallization	54
1.13.1.2	Crystal lattice composition: unit cell and asymmetric unit cell	54
1.13.1.3	X-ray diffractors within crystal lattice produce reciprocal lattice points	55
1.13.1.4	Structural information are stored in reciprocal lattice points	56
1.13.2	X-ray crystallography of <i>PfGST</i>	57
1.13.3	Structural aspects of <i>PfGST</i> complex with hemin and cibacron in anti-malarial design	58
1.14	Objectives	59

CHAPTER 2 - GENETIC CLONING, HETEROLOGOUS	
EXPRESSION, AND PURIFICATION FOR GLUTATHIONE-S-	
TRANSFERASES OF <i>PLASMODIUM FALCIPARUM</i>, HUMAN,	
AND MOUSE	
2.1	Introduction
2.2	Objectives
2.3	Materials and methods

2.3.1	Plasmid extraction and competent cells transformation.....	62
2.3.1.1	Plasmid extraction by alkaline lysis.....	62
2.3.1.2	Chemical transformation of competent cells with plasmid using Transformation and Storage Solution (TSS) 64	
2.3.2	Subcloning and expression of <i>Plasmodium falciparum</i> GST (PfGST).....	64
2.3.2.1	pQE-30-PfGST plasmid propagation and check for gene insertion	65
2.3.2.2	Transformation of M15 cells using pQE-30 and pQE- 30-PfGST plasmids	65
2.3.2.3	Induction of PfGST expression.....	66
2.3.2.4	Subcloning of PfGST gene into pET-16b plasmid	66
2.3.3	RNA extraction, cDNA preparation of human GST Pi-1 (hGSTP1) and subcloning in pCold-I plasmid.....	67
2.3.4	RNA extraction, cDNA preparation of mouse GST Mu-1 (mGSTM1) and subcloning in pCold-I plasmid	69
2.3.4.1	RNA extraction	69
2.3.4.1.1	Total RNA extraction by acid guanidinium thiocyanate phenol-chloroform (GTPC) protocol.....	70
2.3.4.1.2	Total RNA extraction using GeneJet RNA purification kit (Fermentas)	70
2.3.4.1.3	mRNA extraction using Straight A's™ mRNA isolation magnetic bead system (Novagen).....	71
2.3.4.2	Preparation of mGSTM1 cDNA and insertion in pCold plasmid	72
2.3.5	Expression and purification of subcloned GSTs.....	73
2.4	Results and Discussion.....	75
2.4.1	Subcloning and expression of <i>Plasmodium falciparum</i> GST (PfGST).....	75
2.4.1.1	Transformation of M15 cells using pQE-30 and pQE- 30-PfGST plasmids	78
2.4.1.2	Induction of PfGST expression from pQE-30-PfGST plasmid monitored by SDS-PAGE.....	79
2.4.2	cDNA preparation of human GST Pi-1 (hGSTP1) and subcloning in pCold-I plasmid	81
2.4.3	cDNA preparation of mouse GST Mu-1 (mGSTM1) and subcloning in pCold-I plasmid.....	86
2.5	Expression and purification of GSTs	89
2.6	Conclusions	96

CHAPTER 3 - ENZYME KINETICS AND MOLECULAR COMPUTATIONS ARE COPING FOR <i>Pf</i>GST-, hGSTP1-, AND MGSTM1-LIGANDS INTERACTION ASSEMBLY	97
3.1 Introduction	97
3.2 Objectives	98
3.3 Materials and methods	98
3.3.1 Preparation of Buffers, GSH, and CDNB stock solutions	98
3.3.2 Preparation of <i>Pf</i> GST, hGSTP1, and mGSTM1 enzymes stocks	99
3.3.3 Spectrophotometric measurement	100
3.3.3.1 Settings for enzyme kinetic experiments	100
3.3.3.2 Measuring the initial enzyme velocities	102
3.3.4 Determination of GSH and CDNB substrates binding mode to GST	103
3.3.5 Determination of mode of inhibition and kinetic constants	103
3.3.6 Double inhibition studies	104
3.3.7 Molecular docking and energy optimization	104
3.4 Results and discussion	105
3.4.1 Settings for enzyme kinetic experiments	105
3.4.2 Calculation of initial enzyme velocity via 1 st derivative of fitted polynomial equation	106
3.4.3 Determination of <i>K_mGSH</i> and <i>K_mCDNB</i> for <i>Pf</i> GST, hGSTP1, and mGSTM1	108
3.4.4 Determination of the mechanisms for GSH and CDNB mode of binding	111
3.4.5 Determination of experimental <i>K_iGSH</i> and <i>K_iCDNB</i> for known inhibitors and prediction of inter-molecular interaction by molecular docking	114
3.4.5.1 Cibacron blue (CB)	116
3.4.5.2 Ethacrynic acid (EA)	126
3.4.5.3 S-hexyl glutathione (GSX)	132
3.4.5.4 Hemin and Protoporphyrin IX (ProtoIX)	137
3.4.6 Double inhibition of <i>Pf</i> GST to investigate possible interaction between different inhibitors	150
3.4.7 Hemin-HEPES interaction at <i>Pf</i> GST	158
3.4.8 Sulfonamides and <i>Pf</i> GST	163
3.4.9 Conclusions	165
CHAPTER 4 - PLANT SCREENING FOR <i>Pf</i>GST, hGSTP1, AND MGSTM1 INHIBITORS	167

4.1	Introduction	167
4.2	Objectives.....	168
4.3	Methodology	169
	4.3.1 Chemicals, equipment, and preparations	169
	4.3.2 Data analysis	171
4.4	Results and discussion	173
	4.4.1 Determination of enzymes activities and specific activities	174
	4.4.2 Activities of known inhibitors and plant extracts	175
	4.4.2.1 Activities of positive controls	176
	4.4.2.2 Activities of plants extracts.....	179
	4.4.2.2.1 Activities of <i>B. purpurea</i> leaf extracts	179
	4.4.2.2.2 Activities of <i>C. iners</i> bark extracts.....	181
	4.4.2.2.3 Activities of <i>C. furfuracea</i> extracts	182
	4.4.2.2.4 Activities of <i>C. argyratus</i> extracts	183
	4.4.2.2.5 Activities of <i>P. watsonii</i> leaf extracts.....	184
	4.4.2.2.6 Activities of <i>T. catappa</i> leaf extracts.....	185
	4.4.2.2.7 Activities of <i>O. stamineous</i> leaf extracts.....	187
	4.4.2.2.8 Activities of other plant extracts	187
	4.4.2.3 Activities of anti-malarial compounds.....	189
	4.4.3 Mode of inhibition and kinetic constants of <i>Pf</i> GST and mGSTM1 against selected extracts and fractions	193
	4.4.3.1 Inhibition of <i>Pf</i> GST	193
	4.4.3.2 Inhibition of mGSTM1	199
	4.4.3.3 Double inhibition of <i>Pf</i> GST by hemin and plant extracts	203
	4.4.4 Conclusions	205
 CHAPTER 5 - X-RAY CRYSTALLOGRAPHY OF <i>Pf</i>GST- CIBACRON BLUE COMPLEX		207
5.1	Introduction	207
5.2	Objectives.....	209
5.3	Methodology	210
	5.3.1 Materials and reagents	210
	5.3.2 Preparations of protein and crystallization solutions	210
	5.3.3 Crystal growth.....	211
	5.3.4 Data collection	212
	5.3.5 Data processing	212

5.3.5.1	Preparation of structure factor file	212
5.3.5.2	Scaling.....	213
5.3.5.3	Phasing and model refinement	213
5.3.5.4	Ligand fitting.....	214
5.4	Results and discussion	214
5.4.1	Crystallization of <i>Pf</i> GST.....	214
5.4.2	Data processing	218
5.4.2.1	Indexing, cell refinement and integration of diffraction images	218
5.4.2.2	Scaling and merging of reflections by Scala.....	222
5.4.2.3	Analysis of scaled and merged reflections by Xtriage.....	225
5.4.2.4	Phase solution for structure factors by Phaser	227
5.4.2.5	Model refinement	227
5.4.2.6	Fitting CB to electron density map	231
5.4.3	Screening for new crystallization conditions	233
5.5	Conclusion	234
5.6	Recommendations	234

CHAPTER 6 - DEVELOPMENT OF COMPUTER-AIDED *DE NOVO* LEAD DESIGN FOR *Pf*GST INHIBITORS.....

6.1	Introduction	236
6.2	Objectives.....	239
6.3	Experimental design.....	239
6.4	Methodology	241
6.4.1	Software and hardware.....	241
6.4.2	<i>De novo</i> design of <i>Pf</i> GST inhibitors by Isosteric fragments replacements (IFR) approach	243
6.4.3	<i>De novo</i> design of <i>Pf</i> GST inhibitors by Docked fragments replacements (DFR) approach.....	250
6.4.4	Design of <i>Pf</i> GST inhibitors using Structure-Assisted Atom-based <i>De novo</i> molecular design (SAAD) approach.....	254
6.4.4.1	Preparing component functions for genetic algorithm in Matlab2012a.....	254
6.4.4.1.1	Molecule creation functions (population generation).....	256
6.4.4.1.2	Molecules crossover functions (children generation from parents)	258
6.4.4.1.3	Molecules mutation functions (random mutation)	260

6.4.4.1.4	Molecules selection functions	261
6.4.4.1.5	Molecules fitness functions	262
6.4.4.1.6	Main controller function.....	263
6.4.4.2	Application of SAAD for <i>Pf</i> GST inhibitor design.....	265
6.4.5	Design of irreversible <i>Pf</i> GST inhibitor	265
6.4.6	The interaction of GSH, GSX and GLN-CYS moiety to G-site of <i>Pf</i> GST.....	266
6.4.7	Molecular dynamics simulations and free energy calculations.....	266
6.5	Results and discussion	267
6.5.1	Interaction of GSX to G-site of <i>Pf</i> GST	267
6.5.2	<i>De novo</i> fragment-based design of <i>Pf</i> GST inhibitors by Isosteric Fragments Replacements (IFR) approach.....	270
6.5.2.1	GLN-CYS moiety computationally represents GSH in term of interaction energy and mode of binding toward <i>Pf</i> GST	270
6.5.2.2	Segmentation of GLN-CYS moiety into GLN-R and CYS-R query fragments and generation of isosteric fragments replacements.....	277
6.5.2.3	Construction of IFR ligands with global minimum configuration	286
6.5.2.4	Flexible-flexible optimization of Cartesian coordinates and calculation of free energy for protein-ligand interaction by simplified hybrid Molecular Mechanics Poisson-Boltzmann Surface Area (MMPBSA) method.....	298
6.5.2.5	Examples for IFR ligands as <i>Pf</i> GST inhibitors.....	307
6.5.2.5.1	303-IFR	311
6.5.2.5.2	1208-IFR	314
6.5.3	<i>De novo</i> fragment-based design of <i>Pf</i> GST inhibitor using docked fragments replacements (DFR) approach.....	316
6.5.3.1	Fragments preparations	317
6.5.3.2	Construction and processing of DFR ligands	322
6.5.3.3	Flexible-flexible optimization of Cartesian coordinates and calculation of free energy for protein-ligand interaction by simplified hybrid MMPBSA method.....	328
6.5.3.4	Examples of DFR ligands as <i>Pf</i> GST inhibitors.....	331
6.5.3.4.1	1598-DFR.....	335
6.5.3.4.2	2077-DFR	340
6.5.4	Molecular dynamics with AMBER and subsequent free energy calculation with MMPBSA for selected <i>de novo</i> ligands	343
6.5.5	Development and application of SAAD for <i>Pf</i> GST inhibitor design	353

6.5.6	Design of specific irreversible <i>Pf</i> GST inhibitors	359
6.6	Advantages, limitations and suggestions	364
6.7	Conclusions	365
CHAPTER 7 - CONCLUSIONS.....		367
REFERENCES.....		371
APPENDICES		399
Appendix I: Storage of GSTs		
Appendix II: Structure of <i>Pf</i> GST gene in chromosome 14 of <i>Plasmodium falciparum</i> 3D7 isolate		
Appendix III: Sequencing results for <i>Pf</i> GST, hGSTP1 and mGSTM1		
Appendix IV: Plasmids and primer design		
Appendix V: Enzyme kinetics notes		
Appendix VI: Phytochemicals of plant extracts		
Appendix VII: Concentration-response curves for anti-malarial compounds		
Appendix VIII: Determining the concentration of ligand required for co-crystallization experiment		
Appendix IX: Crystal screening hits for <i>Pf</i> GST, <i>Pf</i> GST-GSH and mGSTM1		
Appendix X: Protein crystallization and X-ray crystallography		
Appendix XI: Scala parameters		
Appendix XII: Refmac5 parameters		
Appendix XIII: ProCheck results		
Appendix XIV: Commands used in IFR		
Appendix XV: Molecular dynamics parameter files		
Appendix XVI: Solve problem with mm_pbsa.pl		
Appendix XVII: Letter from Dr. Stefan Ralfs posted with pQE-30- <i>Pf</i> GST		

LIST OF TABLES

	Page
Table 1.1: Enzymes considered as anti-malarial targets (Mehlin, 2005; Buchholz et al., 2007; Alam et al., 2009).	10
Table 2.1: The plasmids and host cells used for cloning and heterologous expression of GSTs in the current study. The name of the supplier company is shown between brackets.....	62
Table 2.2: Origins for chemicals and reagents used in this study	62
Table 2.3: The amino acid sequence of proteins as expressed by the plasmids. The bolded sequence represents amino acids encoded originally by the plasmid, while the other sequence is encoded by the inserted gene.	90
Table 3.1: The K_m (mM) constants for GSH and CDNB toward <i>Pf</i> GST, hGSTP1, mGSTM and hGSTM1.	110
Table 3.2: The binding modes of GSH and CDNB in <i>Pf</i> GST, hGSTP1, and mGSTM1. The values of dissociation constants for GSH and CDNB as well as the interaction factor were obtained from the respected fitted equations.	112
Table 3.3: The kinetic results of <i>Pf</i> GST, hGSTP1 and mGSTM1 using different inhibitors. The values are given as vector represents mode of inhibition, K_i , and alpha values.....	116
Table 3.4: The intermolecular interaction energy terms as calculated by SZYBKI using MMFF94S with flexible protein side chains including flexible polar hydrogen atoms.....	122
Table 3.5: Estimated free energy of binding (kcal/mol) for docked hemin and protoIX conformations	141
Table 3.6: The dissociation constants and interaction factors obtained by fitting the kinetic data to previous equation. All experiments were performed at least in duplicates.....	151
Table 4.1: Activities of GST isoforms measured with standard conjugation reaction of GSH and CDNB.	175
Table 4.2: List for values of IC_{50} , Hill coefficient (h) and percentage of maximum inhibition obtained with positive controls and plant extracts and fractions.....	190
Table 4.3: Comparison between IC_{50} values calculated by curve fitting of concentration response curve, and those back calculated from inhibition constants: for positive controls toward <i>Pf</i> GST.	195

Table 4.4: Mode of inhibition and kinetic constants of plant extracts toward <i>PfGST</i>	195
Table 4.5: Mode of inhibition and kinetic constants of plant extracts toward mGSTM1.....	199
Table 4.6: The interaction between hemin and plant extracts in double-inhibition experiment.....	203
Table 5.1: The results of solvent content analysis by Xtriage.	226
Table 6.1: List of programs involved in this study.	242
Table 6.2: The arrangement of atomic descriptor matrix generated by make_sp2_7ed function.....	257
Table 6.3: The SZYBKI determined energy terms for both of GSH and GLN-CYS moiety against both of monomeric and dimeric forms of <i>PfGST</i>	274
Table 6.4: Comparison between three programs running on CORE™i7 computer regarding GSH and GLN-CYS docking against <i>PfGST</i> dimer. The time is for GSH.	275
Table 6.5: An energy top ranked list of isosteric fragment replacements for GLN-R (first row), showing the energy values as determined by SZYBKI as well as electrostatic shape-Tanimoto (ET) combo. The F atom has been used instead of R atom in order to perform optimization and energy calculation by SZYBKI.	281
Table 6.6: An energy top ranked list of isosteric fragment replacements for CYS-R (first row), showing the energy values as determined by SZYBKI as well as electrostatic shape-Tanimoto (ET) combo. The F atom has been used instead of R atom in order to perform optimization and energy calculation by SZYBKI.	283
Table 6.7: The energy values for optimized, docked and optimized-docked binding modes as calculated by SZYBKI.	294
Table 6.8: Top ranked list of IFR ligands according to value of free energy of binding. GSH and GSX act as controls.	308
Table 6.9: General properties of Molinspiration fragments database including LogP, PSA (polar surface area Å ²), nAtoms (number of atoms), MW (molecular weight), nON (number of oxygen and nitrogen atoms), nOHNA (number of OH and NH groups), nrotb (number of rotatable bonds), and volume of the fragments (Å ³).	318
Table 6.10: The difference in values of Intra MIE terms between bound and free ligand conformers where $\Delta\text{Energy} = \text{Energy}_{\text{bound}} - \text{Energy}_{\text{free}}$	324

Table 6.11: The MMFF94 energy terms calculated for DFR ligands for optimized constructed, docked, and optimized docked modes.	326
Table 6.12: The mean values of entropy terms for free and bound states with respect to IFR and DFR ligands.	330
Table 6.13: Top ranked list of DFR ligands according to value of free energy of binding. GSH and GSX act as controls.	332
Table 6.14: The average values of RMSD and thermodynamic parameters during the production stage of MD simulations.	349
Table 6.15: The free energy composites calculated with MMPBSA from 34 snapshots from MD trajectories of GSH, GSX and 1598-DFR ligands.	352
Table 6.16: List of electrophilic groups that can covalently bound to thiol (Agnew and Gee, 2010).	363

LIST OF FIGURES

	Page
Figure 1.1: Global distribution for percentage of malaria cases caused by <i>Plasmodium falciparum</i> (WHO mapper, 2014).....	5
Figure 1.2: The main classes of anti-malarials. The chemical structures of all the main classes of anti-malarials and other therapeutic and control molecules are assembled according to either the chemical classes they belong to (endoperoxides, 4- and 8- AQs, amino-alcohols) or their function (antifolate, antibiotics), or both (e.g., sulfonamides, a chemical class of antibiotic used in combined anti-malarial therapies) (Delves et al., 2012).	8
Figure 1.3: Summary of the activity of the most widely used anti-malarials throughout the life cycle of <i>Plasmodium</i> . The three main phases, i.e., liver stage, blood stage, and vector stage, of the life cycle of <i>Plasmodium</i> are shown. The two key entry points leading to transmission of the parasites from vector to host and from host to vector are indicated (green circles). Parasite forms specific to each stage are highlighted and drugs identified as inhibitors of development of these forms are listed in boxes and colored as described in previous Figure. Stars highlight components of the main artemisinin combination therapies: green, coartem; red, pyramax; orange, eurartesim; blue, ASAQ (Delves et al., 2012).....	9
Figure 1.4: Classification of functional proteins predicted from <i>Plasmodium falciparum</i> (3D7) genome (Gardner et al., 2002a).	10
Figure 1.5: Structure of tripeptide glutathione (γ -glutamyl-cysteinyl-glycine or GSH).....	12
Figure 1.6: Topology and structural representations of (a) cytosolic GST, (b) mitochondrial GST, and (c) MAPEG. The thioredoxin domain (green) composed from α -helices (circles) and β -sheets (triangles). The C-terminal domain composed mainly from α -helices (Oakley, 2011).....	15
Figure 1.7: Thioredoxin domain common in soluble GSTs; it is composed from 4 beta-sheets interconnected by 3 alpha helices. The GSH binding to GST is stabilized by hydrogen bonds (dashed blue line). The GSH thiol group is activated by giving hydrogen bond to catalytic residue Tyr (Atkinson and Babbitt, 2009).....	15
Figure 1.8: Conjugation reactions catalyzed by rate GST Mu 1-1 (rGSTM1-1, PDB 5FWG) that uses Tyr6 for activating GSH thiol group. The active thiolate group attacks a) phenanthrene epoxide by nucleophilic addition and b) benzylideneacetone double bond by Michaelis addition (Shan and Armstrong, 1994).	18

Figure 1.9: Conjugation reactions catalyzed by GST for a) 1-chloro-2,4-dinitrobenzene (CDNB), b) chlorambucil, c) sulforaphane, d) ethacrynic acid, e) benzylideneacetone, f) phenanthrene epoxide a product of cytochrome P450 catalyzed oxidation of phenanthrene.....	23
Figure 1.10: Reactions catalyzed by GST; a) reduction for cumene, b) <i>o</i> -dopaquinone conjugation, c,d) thiolysis for 4-nitrophenyl acetate and trinitroglycerin, f) isomerization of maleylacetoacetate, f) activation of 1,2-dibromoethane and g) conversion of PGH2 to PGD2).....	24
Figure 1.11: Crystal structure of <i>Pf</i> GST inhibited with GSX (PDB 1Q4J).....	27
Figure 1.12: hGSTP1 bound to EA in a) nonproductive (PDB 2GSS) and b) productive (PDB 3GSS) modes.....	30
Figure 1.13: Superposition of <i>Pf</i> GST (brown, PDB 1Q4J), hGSTP1 (pink, PDB 8GSS), and hGSTM1 (cyan, PDB 1XW6) shows similarity in overall homology (except Mu loop for hGSTM1) as well as the orientation of active site tyrosine residues from (a) Top and (b) bottom views. The ligands shown are S-hexyl glutathione (GSX) for <i>Pf</i> GST and glutathione (GSH) for both of hGSTP1 and hGSTM1.	32
Figure 1.14: Crystal structure of hGSTM1-1 isoform (PDB 1XW6). The hGSTM1-2 isoform has missing two helices (orange). Among human transcriptome, hGSTM1-1 shows the best match (78% sequence similarity) to mGSTM1.	33
Figure 1.15: Structures of GSH analogues.....	36
Figure 1.16: Structures of α , β -unsaturated carbonyl compounds and their epoxide derivatives as well as nitrobenzoxadiazoles as GSTs inhibitors.....	38
Figure 1.17: Structures of natural flavonoids and polyphenols as GSTs inhibitors.....	40
Figure 1.18: Structures of molecules that inhibit GSTs in non-productive (ligand-in) binding mode.....	41
Figure 1.19: The unit cell dimensionality is described by three lengths (a, b, and c) and three angles (α , β , and γ).	55
Figure 1.20: The crystal structure of <i>Pf</i> GST in complex with S-(p-bromobenzyl) glutathione (PDB ID 3FRC) showing the difference electron density map (2mFo-DFc) as mesh up to 2 Å resolution at 2.1 σ . The electron density map is downloaded from electron density server (EDS) and shown together with protein model coordinates using Chimera.	57

Figure 2.1: Schematic representation for a) the map for pQE-30- <i>Pf</i> GST plasmid b) with closer look to the promoter, operator and N-terminal His-tag of cloned <i>Pf</i> GST. The open reading frames are shown as orange arrows.....	77
Figure 2.2: Agarose gel electrophoresis (0.7% w/v agarose) stained with ethidium bromide for a) pQE-30- <i>Pf</i> GST plasmid extracted with TENS (Lane 2) and alkaline lysis protocol (Lane 3), as well as b) the PCR product of pQE-30- <i>Pf</i> GST plasmid using <i>Pf</i> GST specific primers.	78
Figure 2.3: Agarose gel electrophoresis for plasmids extracted from transformed M15 cells, Lane 1: 1kbferm DNA ladder; lane 2-4: three colonies transformed with pQE-30- <i>Pf</i> GST plasmid; Lane 5: a colony transformed with pQE-30 plasmid.....	79
Figure 2.4: Stained gel of SDS-PAGE (12% polyacrylamide) for expression of <i>Pf</i> GST from pQE30- <i>Pf</i> GST plasmid. Lane 1: Pre-stained protein ruler, Lane 2 and Lane 3: non-induced and induced M15 cells, respectively, Lane 4 and Lane 5: non-induced and induced pQE-30/M15 cells, respectively, Lane 6 and Lane 7: non-induced and induced pQE-30- <i>Pf</i> GST/M15 cells, respectively.	80
Figure 2.5: Agarose gel electrophoresis for total RNA extracted (Lane 2) from human blood using GTPC protocol. The amount of RNA loaded on the gel was 50-100 ng.....	81
Figure 2.6: Agarose gel electrophoresis of RT-PCR products. Lane1: GeneRuler™ 1 kb DNA Ladder, Lane 2: product using hGSTP1 specific primers, Lane 3: product using hGSTM1 specific primers.....	82
Figure 2.7: Agarose gel electrophoresis for PCR product of plasmid pools. Lane1: GeneRuler™ 1 kb DNA Ladder, Lane 2-4: PCR product of three pools of plasmids from colonies transformed with pCold-hGSTP1 plasmid.....	84
Figure 2.8: Agarose gel electrophoresis for PCR product using all plasmids from positive pool as templates. Lane1: GeneRuler™ 1 kb DNA Ladder, Lane 2-11: PCR product for individual plasmids. Colony of number one (Lane 2) shows positive insert.....	84
Figure 2.9: Lane 1: GeneRuler™ 1 kb DNA Ladder, Lane 2: digested plasmid from cells showed positive hGSTP1 insert using <i>XhoI</i> and <i>BamHI</i> , Lane3: digested plasmid from cells showed positive pseudo hGSTM2 insert using <i>BamHI</i> and <i>HindIII</i>	84
Figure 2.10: Schematic representation for a) the map for pCold-I-hGSTP1 plasmid b) with closer look to the promoter, operator and N-terminal His-tag of cloned hGSTP1. The open reading frame is shown as orange arrow.	85

Figure 2.11: Agarose gel electrophoresis (0.7% agarose, stained with ethidium bromide) for mouse liver RNA extracts and RT-PCR products of mGSTM1 (~657 bp). Lane 1: VC 1 Kb DNA ladder, Lane 2,3: total RNA extraction using GeneJet, and guanidinium-phenol-chloroform methods, respectively, Lane 4: mRNA extracted using Straight A's™ mRNA Isolation System. Lane 5,6,7: RT-PCR product using each of the previous three RNA extraction methods as a source of template to amplify mGSTM1, respectively.....	87
Figure 2.12: Agarose gel electrophoresis (0.7% agarose, stained with ethidium bromide) for mouse liver RNA extracts and RT-PCR products of mGSTP1. Lane 1:VC 1 Kb DNA ladder, Lane 2: total RNA extraction using GeneJet, kit, Lane3: total RNA extract using guanidinium-phenol-chloroform method, Lane 4: mRNA extracted using Straight A's™ mRNA isolation system. Lane 5,6,7: RT-PCR product using each of the three RNA extraction methods as a source of template to clone mGSTP1, respectively.	87
Figure 2.13: Schematic representation for a) the map for pCold-I-mGSTM1 plasmid b) with closer look to the promoter, operator and N-terminal His-tag of cloned hGSTP1. The open reading frame is shown as orange arrow.	88
Figure 2.14: Purification of <i>Pf</i> GST from TALON eluent using a) size-exclusion chromatography and b) subsequent SDS-PAGE for the collected fractions.....	93
Figure 2.15: Purification of hGSTP1 from TALON eluent using a) size-exclusion chromatography and b) subsequent SDS-PAGE for the collected fractions.....	94
Figure 2.16: Purification of mGSTM1 from TALON eluent using a) size-exclusion chromatography and b) subsequent SDS-PAGE for the collected fractions. The monomer peak (yellow) is overridden by the contamination peak in SEC, however, it appears in SDS-PAGE.....	95
Figure 3.1: The arrangement of 96-well plate to accommodate duplicate of enzymatic assay of variable substrate and inhibitor to determine <i>K_i</i> constant.....	101
Figure 3.2: Fitting the 4 th polynomial function $y = a + bx + cx^2 + dx^3 + ex^4$ to sample data for different concentrations of substrate (highest to lowest, 1 to 8) where a variable is a) unconstrained, b) shared and less than the smallest <i>x</i> value in the set c) constrained to zero before blank subtraction, and d) constrained to zero after blank subtraction.	107

Figure 3.3: The effect of HEPES content on <i>Pf</i> GST activity. HEPES activates <i>Pf</i> GST and reduces the lag phase.	109
Figure 3.4: Fitting the equation of compulsory-order mechanism to kinetic data of a) <i>Pf</i> GST, and random-ordered mechanism to b) hGSTP1 and c) mGSTM1.....	113
Figure 3.5: Superimposed crystal structures of hGSTP1 in complex with GSH (PDB 8GSS, gold), GS-DNB (PDB 18GS, magenta), and CB (PDB 20GS, blue). The anthraquinone moiety of CB overlapped with CDNB but not with GSH binding sites.	118
Figure 3.6: The crystal structure of hGSTP1 in complex with CB. The anthraquinone moiety of CB for docked conformation (green) is completely overlapped with the crystal conformation (magenta). The side chains of Tyr7 and Arg13 establish four hydrogen bonds with the carbonyl, sulfonic and amino groups of anthraquinone moiety. However, both of sulfophenyl groups and the triazino secondary amine group of docked DSPT moiety establish extra three hydrogen bonds with Thr109 side chain. Hydrogen bonds are shown as green lines.	119
Figure 3.7: Docked conformation of CB (blue sticks) at <i>Pf</i> GST showing the established hydrogen bonds (green lines).....	119
Figure 3.8: The binding mode of docked cibacron blue (green) at the H and G-sites of hGSTP1 and <i>Pf</i> GST, respectively. The docked and crystal conformations (magenta) of anthraquinone moiety of cibacron blue are overlapped in hGSTP1. The Inter-molecular H-bonds (green lines) and interaction energies (calculated by SZYBKI) for anthraquinone and disulphophenyl triazine moieties are shown.	122
Figure 3.9: Lineweaver-Burk plot for <i>Pf</i> GST inhibition by CB using GSH and CDNB as variable substrates.	123
Figure 3.10: Lineweaver-Burk plot for hGSTP1 inhibition by CB using GSH and CDNB as variable substrates.	124
Figure 3.11: Lineweaver-Burk plot for mGSTM1 inhibition by CB using GSH and CDNB as variable substrates.	125
Figure 3.12: The crystal structure of hGSTP1 in complex with EA (PDB 3GSS) showing oxygen atom of crystal water molecules (red spheres) which are involved in maintaining network of hydrogen bonds (green dashed lines) between ligand and the protein.....	127
Figure 3.13: Lineweaver-Burk plot for <i>Pf</i> GST inhibition by EA using GSH and CDNB as variable substrates.	129
Figure 3.14: Lineweaver-Burk plot for hGSTP1 inhibition by EA using GSH and CDNB as variable substrates. Due to strong inhibition of hGSTP1 at 180 μ M of EA and low concentrations of CDNB,	

deviation from linearity is observed upon determination of <i>KiCDNB</i> .	130
Figure 3.15: Lineweaver-Burk plot for mGSTM1 inhibition by EA using GSH and CDNB as variable substrates.	131
Figure 3.16: Crystal structure of hGSTP1 with GSX (PDB 9GSS, brown) superimposed on asymmetric unit cells for <i>Pf</i> GST dimer (PDB 2AAW, magenta) and tetramer (PDB 1Q4J, cyan). The S-hexyl tail accommodates different orientation in each crystal. In hGSTP1, the tail is descending down toward the loop connecting β 1 and α 1 of thioredoxine domain. While in <i>Pf</i> GST, the tail is directed toward the inner (cyan) or outer (magenta) sides of H-site. Note that PEG330 molecule occupied distal part of the H-site in 2AAW.	133
Figure 3.17: Lineweaver-Burk plot for <i>Pf</i> GST inhibition by GSX using GSH and CDNB as variable substrates.	134
Figure 3.18: Lineweaver-Burk plot for hGSTP1 inhibition by GSX using GSH and CDNB as variable substrate.	135
Figure 3.19: Lineweaver-Burk plot for mGSTM1 inhibition by GSX using GSH and CDNB as variable substrate.	136
Figure 3.20: Docking of hemin to <i>Pf</i> GST reveals two binding sites (a); A-site which is overlapped with H-site (b), and B-site which is overlapped with HEPES binding site of hGSTP1.	140
Figure 3.21: Docked conformations of hemin toward hGSTP1 in (a) presence and (b) absence of GSH at G-site. The crystal conformation of GSH (blue) was shown in b to describe the overlap with docked hemin at G-site.	143
Figure 3.22: Structure of hGSTP1 with hemin (red) docked to B-site. Note that docked hemin at B-site has no direct interaction with the C-terminal tail and, consequently, improbable allosteric effect on H-site.	143
Figure 3.23: Lineweaver-Burk plot for <i>Pf</i> GST inhibition by hemin using GSH and CDNB as variable substrates. The readings at low CDNB concentrations were omitted because of inaccuracy in absorbance measurements at 3 μ M of hemin.	144
Figure 3.24: Lineweaver-Burk plot for hGSTP1 using GSH and CDNB as variable substrates.	145
Figure 3.25: Lineweaver-Burk plot for mGSTM1 using GSH and CDNB as variable substrates. The non-linearity at low CDNB and GSH concentrations in the presence of high concentration of hemin may be due to cooperativity.	146

Figure 3.26: Lineweaver-Burk plot for pfGST inhibited by protoIX using GSH and CDNB as variable substrates.	147
Figure 3.27: Lineweaver-Burk plot for mGSTM1 inhibited by protoIX using GSH and CDNB as variable substrates.	148
Figure 3.28: Enzyme kinetic and molecular docking experiments cooperate to build the interaction models for GSX (green), CB (cyan), hemin (red), EA (yellow) at each of <i>Pf</i> GST, hGSTP1 and mGSTM1. The crystal structure of hGSTM1 bound to GSH (pink) is shown instead of mGSTM1 (unavailable crystal structure).	149
Figure 3.29: Double inhibition experiments between hemin on one side and (a) CB, (b) EA, and (c) GSX on the other side.	152
Figure 3.30: Double inhibition experiments between EA on one side and (a) CB (b) GSX on the other side, and (c) between GSX and CB.	153
Figure 3.31: Lineweaver-Burk plot for <i>Pf</i> GST inhibited by hemin in the presence of 50 μ M of EA upon using variable GSH and CDNB concentrations.	155
Figure 3.32: Minimization of GS-EA (magenta) and GS-DNB (green) molecules within G and H-sites of <i>Pf</i> GST. The docked conformation of hemin (orange) which is obtained in the presence of GSH at G-site is shown.	157
Figure 3.33: Schematic representation of inhibitors binding in <i>Pf</i> GST according to kinetic and docking results. The molecules are GSH (dark pink), CDNB (yellow), CB (blue), GSX (magenta), GS-EA (green), and hemin (red).	157
Figure 3.34: Structure of 4-(2-hydroxyethyl)-1-piperazineethanesulfonic acid (HEPES).	159
Figure 3.35: Non-competitive equation fitted to the kinetic data of <i>Pf</i> GST inhibition by HEPES using variable GSH and CDNB substrates. No obvious inhibition was observed using up to 200 mM of HEPES.	160
Figure 3.36: Fitting the double inhibitor equation to initial velocity measurements at different HEPES and hemin concentrations. The measurements were recorded for standard GSH-CDNB reactions using <i>Pf</i> GST tetrameric form pre-incubated with (a) HEPES and (b) hemin.	161
Figure 3.37: The docked HEPES conformation at <i>Pf</i> GST (blue stick) interacts with the C-terminal tail as well as the loop connecting α -1 and β -2 through several hydrogen bonds (green lines). The interlock (red oval) used during tetramerization was shown by superimposing one unit of <i>Pf</i> GST dimer (brown, PDB 2AAW) against the tetrameric form (cyan, PDB 1OKT).	163

Figure 3.38: Sulfa drugs which have been tested for GST activity.	164
Figure 4.1: The arrangement of 96-well plate to accommodate duplicates of IC ₅₀ measurements toward <i>Pf</i> GST, hGSTP1, and mGSTM1. A duplicate of blank measurement (no enzyme) was used as a reference for all enzymes duplicates.	170
Figure 4.2: Docked conformations of CB at both subunits of hGSTP1 dimer.	177
Figure 4.3: GSTs inhibition assays using cibacron blue, hemin, and ethacrynic acid as positive controls.	178
Figure 4.4: GSTs inhibition assays using <i>Bauhinia purpurea</i> leaves	180
Figure 4.5: GSTs Inhibition assay using <i>Cinnamomum iners</i> bark extracts v	182
Figure 4.6: GSTs inhibition assays using <i>Chaenotheca furfuracea</i> extracts	183
Figure 4.7: GSTs inhibition assays using <i>Croton argyratus</i> extracts.	184
Figure 4.8: GSTs inhibition assays using <i>Phyllanthus watsonii</i> extracts	185
Figure 4.9: GSTs Inhibition assay using <i>Terminalia catappa</i> leaf extracts	186
Figure 4.10: GSTs inhibition assays using <i>Orthosiphon stamineous</i> extracts	187
Figure 4.11: GSTs inhibition assays using <i>Andrographis paniculata</i> , <i>Eurycoma</i> <i>longifolia</i> and <i>Mitragyna speciosa</i> extracts.	188
Figure 4.12: A summary for overall activity of plant extracts and fractions toward each of <i>Pf</i> GST, hGSTP1, and mGSTM1.	192
Figure 4.13: Lineweaver-Burk plot for <i>Pf</i> GST inhibition by n-butanol fraction of <i>Cinnamomum iners</i> using GSH and CDNB as variable substrates	196
Figure 4.14: Lineweaver-Burk plot for <i>Pf</i> GST inhibition by methanol fraction of <i>Phyllanthus watsonii</i> using GSH and CDNB as variable substrates	197
Figure 4.15: Lineweaver-Burk plot for <i>Pf</i> GST inhibition by n-butanol fraction of <i>Terminalia catappa</i> using GSH and CDNB as variable substrates	198
Figure 4.16: Lineweaver-Burk plot for mGSTM1 inhibition by n-butanol fraction of <i>Cinnamomum iners</i> using GSH and CDNB as variable substrates.	200
Figure 4.17: Lineweaver-Burk plot for mGSTM1 inhibition by methanol fraction of <i>Phyllanthus watsonii</i> using GSH and CDNB as variable substrates	201

Figure 4.18: Lineweaver-Burk plot for mGSTM1 inhibition by n-butanol fraction of <i>Terminalia catappa</i> using GSH and CDNB as variable substrates	202
Figure 4.19: Double inhibition of <i>PfGST</i> by hemin and each of <i>C. iners</i> (n-butanol frac.), <i>P. watsonii</i> (methanol ext.), and <i>T. catappa</i> (n-butanol frac.).....	204
Figure 5.1: Crystallized <i>PfGST</i> (a) without ligand, (b) with CB, and (c) with hemin. For b and a, the drops on left obtained using Harwaldt et al. (2002) condition, while on right using the modified condition. (note larger crystals were obtained).	217
Figure 5.2: First diffraction image recorded for <i>PfGST</i> -CB crystal with reciprocal lattice spots (top) before and (bottom) after indexing, refinement of unit cell dimensions and beam center. The blue, yellow, red and green boxes surrounds full, partial, overlaps and wide reflection spots, respectively. The beam stopper was masked by green circle.	220
Figure 5.3: Integration of spots by iMoslm for 144 diffraction images shows the mean of $I/\sigma(I)$ ($\langle I/\sigma(I) \rangle$) for profile fitted intensities (pf) and summation integration intensities (sum) for each of partial (par), full (full) and higher resolution bin (HR) reflections. Note the absence of full reflection intensities in all diffraction images.....	221
Figure 5.4: Independent measurement of mosaicity as well as the missetting angles of $\phi(x)$, $\phi(y)$ and $\phi(z)$ for the 144 diffraction images.	221
Figure 5.5: The measurement of detector Tilt and Twist as well as the RMS error in spots positions over all diffraction images.	222
Figure 5.6: The structure factors from 0kl planes produced by iMosflm (a) before and (b) after scaling and merging of reflections using SCALA. The darkness of black spots measures the intensities while the blue spots are predicted. Spots are shown up to the resolution of 1.89 Å. The Figures are produced by ViewHKL 1.04 from CCP4.....	224
Figure 5.7: The averaged signal-to-noise ratio of intensity ($\langle I/\sigma(I) \rangle$) and <i>Rmerge</i> for all reflections in each of the 144 diffraction images as processed by Scala.	225
Figure 5.8: Analysis of scaled and merged reflections by Xtriage showing a) average signal to noise ratio and b) completeness and data strength.	226
Figure 5.9: Refinement cycles showing the progression of R-work and R-free.....	229
Figure 5.10: Refinement cycles showing the progress in mean RMSD of bonds lengths (rmsBOND), angles (rmsANGL) and chiral volumes (rmsCHIRAL) during refinement relative to original states.	

While deviations of bond lengths and angles from ideal values are provide as Z-scores of zBOND and zANGL, respectively.	229
Figure 5.11: Ramachandran plot for Phi (ϕ or horizontal axis f) and Psi (ψ or vertical axis y) for all (General), Proline-Proline bound (Pro-Pro), Proline and Glycine amino acids.	230
Figure 5.12: The refined model for <i>Pf</i> GST showing the electron density map ($2F_0 - F_c$, $\sigma = 0.7$) for the active site of one subunits (red box). Two views for CB (magenta sticks) tried to fit the unoccupied regions of the electron density map.	232
Figure 6.1: Schematic representation for the approaches developed and applied to design reversible and irreversible <i>Pf</i> GST inhibitors	240
Figure 6.2: The approaches involved in fragment-based design of <i>Pf</i> GST inhibitors are: Isosteric Fragment Replacement (IFR) and Docked Fragment Replacement (DFR).	241
Figure 6.3: The structures of GLN-R and CYS-R fragments that are used as template for isosteric fragments search.	243
Figure 6.4: Grid box for docking of <i>de novo</i> designed ligands covers the whole GSH (shown in CPK model) binding site in a <i>Pf</i> GST dimer.	248
Figure 6.5: Scheme for fragment-based <i>de novo</i> design of <i>Pf</i> GST inhibitor using isosteric-fragment replacement approach. The programs used for each step are provided between brackets.	249
Figure 6.6: Fragments database were docked with FRED at both of site-1 (red box) and site-2 (yellow box). The two boxes are overlapped at main chain carboxylic carbon of Cysteine residue of crystal <i>GSX</i> (arrow), where a hypothetical sphere (cyan) was allocated to restrain fragments R atom position during docking.	250
Figure 6.7: Scheme for fragment-based <i>de novo</i> design of <i>Pf</i> GST inhibitor using docked fragment replacements approach. The programs used for each step are provided between brackets.	253
Figure 6.8: Schematic representation of gene composites that encodes full molecular structure. The gene is composed from three matrices, namely: atomic descriptors, position coordinates, and quaternion angles.	255
Figure 6.9: A schematic representation of the four stages as well as the main and sub functions used in genetic algorithm for Structure-Assisted Atom-based <i>De novo</i> molecular design (SAAD).	256
Figure 6.10: Example of molecules created by four calls of <code>make_sp2_7ed</code> function using total number of atoms equal to 20. Note that all molecules are flat, composed from almost sp^2 hybridized carbon	

	atoms geometry, and have master atom at 0,0,0 coordinates (encircled).....	258
Figure 6.11:	Crossover between Mol1 and Mol2. The <code>crossover_mol_2ed</code> function randomly connects atoms from Mol1 (blue stick) and Mol2 (red stick) to generate child molecule (green stick).	259
Figure 6.12:	The parent molecule (blue stick) was mutated by <code>mutation_mol_2ed</code> function to give mutated molecule (green stick).	261
Figure 6.13:	a) The graphical interface of SAAD program showing the progress of molecular evolution. As shown, the fitness value (binding energy) is reduced to lower value within the first few generations due to progression in molecular structure optimization. b) An atomic representation of <i>Pf</i> GST (light blue dots) with grid box (dark blue dots) covers the binding pocket where color of the dot encodes the electrostatic potential for probe atom of charge=+1.....	264
Figure 6.14:	The G-site of <i>Pf</i> GST shown as a) 3D representation occupied with <i>S</i> -hexylglutathione (GSX): the Lys15 and Gln58 residues divide the site into two subsites (site-1 and site-2), and b) overlapped 2D representation for bound glutathione (GSH, blue) and GSX (gray colored) at the G-site of <i>Pf</i> GST dimer showing hydrogen bonds (dashed line), VdW and hydrophobic interactions (radiated red lines). Interactions between GSH and amino acids are labeled in green while interactions between GSX and amino acids are labeled in gray.	269
Figure 6.15:	The crystal structure of GSH at G-site of a) hGSTP1 (PDB 8GSS) and b) <i>Pf</i> GST (PDB 2AAW). The Gly residue of GSH (red circled) establishes three hydrogen bonds with Gln51, Lys44, and Trp38 in hGSTP1, while none in <i>Pf</i> GST. H-bonds are detected within 2.5 Å between donors and acceptors without angle consideration. The carbon atoms of next subunit in the dimer are colored yellow. Note, only GSH moiety of GSX is shown for <i>Pf</i> GST.	272
Figure 6.16:	Docking of a) GSH and b) GLN-CYS portions of crystal GSX (gray) back to G-site of <i>Pf</i> GST dimer using VINA (magenta), AUTODOCK4.2 (yellow), and FRED (green). The amino acids of the next subunit of <i>Pf</i> GST dimer are shown as spheres.....	276
Figure 6.17:	Representatives of GLN-F replacements produced by BROOD according to combo score of a) shape Tanimoto and b) electrostatic field. Ring inclusion has been used to constraint BROOD search. The electrostatic field of F atom (green) is shown; however, it was not used for electrostatic field similarity scoring, yet only used for shape Tanimoto scoring.	278

Figure 6.18: Representatives of CYS-F replacements produced by BROOD according to combo score of a) shape Tanimoto and b) electrostatic field. Ring inclusion has been used to constraint BROOD search. The electrostatic field of F atom (green) is shown; however, it was not used for electrostatic field similarity scoring, yet only used for shape Tanimoto scoring.	279
Figure 6.19: Scatter plots for electrostatic shape-Tanimoto (ET) combo score versus Inter MIE.	286
Figure 6.20: Histogram showing the distribution of synthetic accessibility score among IFR ligands.	287
Figure 6.21: Two fragments represent isosteric replacements of GLN-R and CYS-R are checked for R atom (cyan) overlap and P-R-P angle (green).	288
Figure 6.22: The contribution of VdW and electrostatic interactions to the final Inter MIE for IFR ligands as well as the effect of Intra MIE on the final energy score.	290
Figure 6.23: Histogram showing the frequencies of Intra MIE and Inter MIE in the IFR ligands.	290
Figure 6.24: Scatter plots for values of a) Intra MIE and b) Inter MIE determined using MMFF94 (SZYBKI) for optimized versus docked ligands conformers, as well as c) histograms for deviation in binding configurations.	292
Figure 6.25: The fluctuation in VdW and electrostatic potentials with respect to increase in Inter MIE for both of a) FRED and b) VINA docked modes.	294
Figure 6.26: Comparisons between optimized and docked-optimized configurations are shown with respect to values of a) Inter MIE and b) RMSD.	295
Figure 6.27: The calculated free energy of IFR ligands is shown a) histogram, b) with the concomitant fluctuation of enthalpy, desolvation and entropy terms, and c) the change in internal ligand strain upon binding.	304
Figure 6.28: The concomitant fluctuation in total configurational, partial ligand solvation, and protein desolvation entropy values with respect to final entropy (TS) of bound IFR ligand.	306
Figure 6.29: The concomitant fluctuation in total configurational, partial ligand solvation, and protein desolvation entropy values with respect to final entropy (TS) of free IFR ligand.	306

Figure 6.30: Scatter plot show the correlation between change in ligand solvation entropy upon binding and fraction of ligand surface exposed to solvent.	307
Figure 6.31: The structure of 303-IFR ligand and the constituent fragments.	311
Figure 6.32: The interaction of 303_IFR_31_260 (or 303-IFR) with G-site of <i>Pf</i> GST. The top diagram shows 2D representation of inter-molecular interactions using dashed green lines for hydrogen bonds and radiated lines for VdW and hydrophobic interactions. The bottom Figure shows 3D stereo view including inter-molecular H-bonds (green dashed lines) and Pi stacking (orange lines).	313
Figure 6.33: The structure of 1208-IFR ligand and the constituent fragments.	314
Figure 6.34: The interaction of 1208_IFR_122_176 (or 1208-IFR) with G-site of <i>Pf</i> GST. The top diagram shows 2D representation of inter-molecular interactions using dashed green lines for hydrogen bonds and radiated lines for VdW and hydrophobic interactions. The bottom Figure shows 3D stereo view including inter-molecular H-bonds (green dashed lines) and Pi stacking (orange lines).	315
Figure 6.35: The GSH binding site of <i>Pf</i> GST with fragments docked against site-1 (green stick) and site-2 (yellow stick). The substitution atom (R) of docked fragments was constrained to be within a hypothetical sphere of 1 Å radius (cyan).	318
Figure 6.36: The fluctuation in physicochemical properties of fragments docked to site-1 with respect to improvement in Chemgauss4 score. The horizontal axis represents fragment number while the vertical axis represents the value of the measured property.	319
Figure 6.37: The fluctuation in physicochemical properties of fragments docked to site-2 with respect to improvement in Chemgauss4 score. The horizontal axis represents fragment number while the vertical axis represents the value of the measured property.	320
Figure 6.38: Scatter plots of Chemgauss4 score vs. each of molecular weight (MW), polar surface area (PSA), calculated LogP (cLogP) and total number of hydrogen bond donors and acceptors (nHD+nHA) with respect to fragments docked to site-1 and site-2. Note: only fragments which bind to site-1 were involved (i.e. have Chemgauss4 score <0).	322
Figure 6.39: Histogram showing the distribution of synthetic accessibility score among DFR ligands.	323
Figure 6.40: The energy terms calculated by SZYBKI during Cartesian coordinates optimization of IFR ligands within G-site of <i>Pf</i> GST shown as a) fluctuation in relation to the Inter MIE and as b)	

histograms for inter MIE and internal molecular strain developed due to binding.	325
Figure 6.41: The energy terms calculated by SZYBKI during Cartesian coordinates optimization of docked IFR ligands within G-site of <i>Pf</i> GST shown as a) fluctuation in relation to the Inter MIE, b) histograms for inter MIE and internal molecular strain developed due to binding, and c) the deviation in binding mode measured by RMSD (Å) following optimization and docking.	327
Figure 6.42: The calculated free energy of DFR ligands is shown as a) histogram, b) with the concomitant fluctuation of enthalpy, desolvation and entropy terms, and c) the change in internal ligand strain upon binding.	329
Figure 6.43: The fluctuation of individual entropy terms and their contribution to the final entropy (TS) for free and bound DFR ligands.	331
Figure 6.44: The structure of 1598-DFR and the constituent fragments.	336
Figure 6.45: The interaction of 1598-DFR with G-site of <i>Pf</i> GST. The top diagram shows 2D representation of inter-molecular interactions using dashed green lines for hydrogen bonds and radiated lines for VdW and hydrophobic interactions. The bottom Figure shows 3D stereo view including inter-molecular H-bonds (green dashed lines) and Pi stacking (orange lines).	337
Figure 6.46: The structure of one subunit of <i>Pf</i> GST dimer showing the G-site with overlapped structures of 1598-DFR (gray) and GSH moiety of crystal GSX (green).	339
Figure 6.47: The crystal structure of hGSTP1 in complex with GSH at G-site (carbon colored gray) and sulfasalazine at H-site (carbon colored yellow)	339
Figure 6.48: The structure of 2077-DFR and the composite fragments	341
Figure 6.49: The interaction of 2077_DFR_980_5760 (or 2077-DFR) with G-site of <i>Pf</i> GST. The top diagram shows 2D representation of inter-molecular interactions using dashed green lines for hydrogen bonds and radiated lines for VdW and hydrophobic interactions. The bottom Figure shows 3D stereo view including inter-molecular H-bonds (green dashed lines) and Pi stacking (orange dashed lines).	342
Figure 6.50: The structure of one subunit of <i>Pf</i> GST dimer showing the G-site with overlapped structures of 2077-DFR (gray) and GSH moiety of crystal GSX (green).	343
Figure 6.51: The change in a) temperature, b) pressure, c) volume and d) density of the periodic box as derived from trajectories of MD simulations.	347

Figure 6.52: The fluctuation in values of a) kinetic energy ($E_{K_{TOT}}$), b) potential energy ($E_{P_{TOT}}$) and c) total energy ($E_{TOT}=E_{K_{TOT}}+E_{P_{TOT}}$) calculated for trajectories of MD simulations.	348
Figure 6.53: The RMSD relative to original state for a) receptor backbone atoms (N, CA, C) and b) ligand heavy atoms.	349
Figure 6.54: The application of SAAD for designing molecule composed from 10 atoms using grid box at gamma-glutamyl part of GSH (a). Through 30 generations, the algorithm ended with molecules of -4.3 kcal/mol (b). The generated molecule (thick stick) has structure and atomic composition close to gamma-glutamyl moiety of GSH (thin stick) (c).	355
Figure 6.55: The effect of population size on the SAAD outcome upon fixing other parameters as Generations=30, Mutation rate=0.2, Crossover fraction=0.8, Crossover E weight=0.9, Survived elites=30, O atoms %=10, and percentage of N atoms %=10. Increasing the population size usually (but not certainly) lead to molecules of better interaction energy and higher number of heteroatoms composites.	356
Figure 6.56: The application of grid sub-boxes approach in SAAD. The binding site of GSX is a) encompassed by a grid box which was computationally divided into two sub-boxes during molecular design process in order to generate b) two molecules of 10 atoms each.	358
Figure 6.57: The crystal structures of human GSTs of a) Zeta (PDB 1FW1), b) Theta (isoform 1-1, PDB 2C3N), c) Omega (isoform 2, PDB 3Q18), d) Pi (isoform 1-1, PDB 8GSS), and e) <i>Pf</i> GST (PDB 2AAW).	361
Figure 6.58: Crystal structure of a) hGSTP1-1 with bound GSH (PDB 8GSS) and b) <i>Pf</i> GST with bound S-hexylglutathione (PDB 2AAW). The distance as green line is shown between α amine group of γ -glutamyl residue of the ligands and the closest Cys residues on subunits A and B of the dimer.	362
Figure 6.59: Proposed irreversible <i>Pf</i> GST inhibitors.	363

LIST OF SYMBOLS

ΔA_{blank}	Change in absorbance for blank
ΔA_{sample}	Change in absorbance for sample
ΔG_{GB}	Total free energy using MMGBSA (GBTOT-TSTOT)
ΔG_{PB}	Total free energy using MMPBSA (PBTOT-TSTOT)
$[E]$	Enzyme concentration
IC_{50}	The concentration produces 50% inhibition
K_{cat}	Rate constant for enzyme catalysis
K_d	Rate constant for dissociation of enzyme-inhibitor complex
K_i	Rate constant for enzyme inhibition
K_i^{CDNB}	Inhibitory constant for enzyme inhibition measured by varying inhibitor and CDNB concentrations
K_i^{GSH}	Inhibitory constant for enzyme inhibition measured by varying inhibitor and GSH concentrations
K_m	Concentration of substrate that occupied 50% of enzyme binding sites.
K_m^{CDNB}	Concentration of CDNB to achieve half of maximum enzyme velocity
K_m^{GSH}	Concentration of GSH to achieve half of maximum enzyme velocity
$[S]$	Substrate concentration
v	Enzyme velocity
v_i	Initial enzyme velocity
V_{max}	Maximum enzyme velocity
v_o	Maximum enzyme velocity

LIST OF ABBREVIATIONS

A	Adenine
Å	Angstrom
AM1-BCC	Semi-empirical (AM1) with bond charge correction (BCC)
<i>A. paniculata</i>	<i>Andrographis paniculata</i>
<i>B. purpurea</i>	<i>Bauhinia purpurea</i>
BLAST	Basic Local Alignment Search Tool
bp	Base pair. Usually used for DNA size
BSA	Bovine serum albumin
C	Cytosine
<i>C. argyratus</i>	<i>Croton argyratus</i>
<i>C. furfuracea</i>	<i>Chaenotheca furfuracea</i>
<i>C. iners</i>	<i>Cinnamomum iners</i>
CB	Cibacron blue
CDNB	1-chloro-2,4-dinitrobenzene
DEPC	Diethylpyrocarbonate
DFR	Docked-Fragment Replacement
dH ₂ O	Distilled water
DMSO	Dimethyl sulfoxide
dNTP	Deoxynucleotide phosphate
DSPT	Disulphophenyl triazine
<i>E. longifolia</i>	<i>Eurycoma longifolia</i>
EA	Ethacrynic acid
ELE	Electrostatic potential energy
G	Guanine
GAS	Inter-Molecular Interaction energy in gas phase
GB	Generalized Born
GBCAL	Reaction field energy calculated by GB
GBELE	Electrostatic contribution to total free energy (GBCAL + ELE)
GBLIP	Hydrophobic contribution to total free energy (GBSUR + VDW)
GBSOL	Desolvation energy (GBSUR + GBCAL)
GBSUR	Hydrophobic contrib. to solv. free energy for GB calculations
GBTOT	Total enthalpy contribution of free energy (GBSOL + GAS)
GS-DNB	<i>S</i> -(2,4-dinitrobenzyl) glutathione
GS-EA	Glutathione-ethacrynic acid conjugate
GSH	Glutathione
G-site	Glutathione binding site
GST	Glutathione- <i>S</i> -transferase
GSX	<i>S</i> -hexyl glutathione
<i>h</i>	Hill slope
<i>H</i>	Hill coefficient
HEPES	4-(2-hydroxyethyl)-1-piperazineethanesulfonic acid
hGSTP1	Human Glutathione- <i>S</i> -transferase Pi-1
HOMO	Higher occupied molecular orbital

H-site	Hydrophobic binding site
IFR	Isosteric-Fragments Replacement
Inter MIE	Inter-Molecular Interaction energy (or GAS)
Intra MIE	Intra-Molecular Interaction Energy (or INT)
IPTG	Isopropyl β -D-1-thiogalactopyranoside
JNK	C-Jun N-terminal Kinase
U	International unit for enzyme activity represent number of μ M of product fprmed per minute per ml (μ M/min/ml)

**PENGKLONAN MOLEKUL, UNGKAPAN DAN PENCIRIAN
GLUTATHIONE-S-TRANSFERASE SEBAGAI SASARAN NOVEL
BAGI REKABENTUK UBAT-UBATAN DAN PENEMUAN
ANTIMALARIA**

ABSTRAK

Glutathione-S-transferase (GSTs) adalah sekumpulan enzim detoksifikasi. *Plasmodium falciparum* mempunyai isoform tunggal GST (PfGST) yang terlibat dalam bagi detoksifikasi heme. Isoform GSTs daripada manusia (hGSTP1) dan tikus (mGSTM1) terlibat dalam tekanan apoptosis laluan kinase dan menjadi pengantara bagi kerintangan sel kanser terhadap kemoterapi. PfGST, hGSTP1 dan mGSTM1 telah berjaya diklon dan diungkapkan secara heterologus dalam *E. coli*. Eksperimen perencatan, kinetik dan penghabluran enzim telah dijalankan untuk mencari sebatian yang berpotensi untuk merencat PfGST. Substrat PfGST iaitu glutathione (GSH) dan 1-kloro-2,4-dinitrobenzena (CDNB), serta perencat glutathione yang diketahui iaitu S-hexyl (GSX), cibacron biru (CB), asid etacrinic asid (EA), Hemin, protoporphirin IX (protoIX) dan 4-(2-hidroxiethyl)-1 asid-piperazineetanesulfonik (HEPES) telah dikaji. Keputusan menunjukkan afiniti, mod pengikatan dan interaksi yang mungkin antara perencat dan PFGST. Dua tapak pengikatan telah dicadangkan untuk Hemin dalam PfGST. Bagaimanapun CB, GSX, EA dan HEPES tidak mampu bersaing dengan Hemin untuk mengeluarkannya daripada tapak pengikatannya dan menjadikan mereka tidak sesuai untuk digunakan sebagai petunjuk. Oleh kerana afiniti yang tinggi dan interaksi yang mungkin antara CB dan Hemin, struktur kristal kompleks CB dengan PfGST dikaji menggunakan X-ray kristalografi. Sebagai satu pendekatan alternatif untuk mendapatkan petunjuk, molekul telah direka untuk menyasarkan tapak pengikat

GSH dalam *PfGST* dan menjejaskan kestabilan Hemin untuk mengikat. Peneraju berdasarkan molekul GSH dan / atau poket pengikatannya telah dicari menggunakan pendekatan *de novo*. Tiga pendekatan telah dibangunkan untuk perencat berbalik menggunakan reka bentuk berasaskan serpihan dan reka bentuk berasaskan atom, dan satu reka bentuk menggunakan pendekatan untuk perencat tidak berbalik. Penggantian serpihan-isosterik (IFR) dan penggantian serpihan-berlabuh (DFR) telah berjaya menjana ligan *de novo* dengan tenaga bebas untuk mengikat dan skor akses sintetik telah dinilai untuk pemilihan penunjuk. Simulasi dinamik molekul menunjukkan bahawa 1598-DFR mengekalkan kestabilan untuk mengikat dengan pengikatan tenaga bebas adalah -16 Kcal / Mol dan RMSD berfungsi kurang daripada 3 Å sepanjang tempoh simulasi (7.5 ns). Pendekatan ketiga yang menjana molekul penunjuk oleh pemasangan atom menggunakan reka bentuk molekul *de novo* berasaskan atom bantuan struktur (SAAD) yang khusus membuatkan serpihan molekul muat untuk poket pengikatan γ -glutamil moiti GSH. Dalam pendekatan terakhir, perencat tidak berbalik telah direka untuk membentuk ikatan kovalen dengan *PfGST* dengan menggunakan susunan unik 3 dimensi sisa sisteina. Analog-analog telah direka untuk mewujudkan ikatan kovalen dengan Cys101 melalui moiti elektrofilik yang menggantikan α -amino γ -glutamil GSH. Molekul penunjuk yang telah direka boleh membuka saluran baru untuk merawat malaria melalui perencatan *PfGST* berbalik dan tidak berbalik. Ekstrak tumbuhan telah disaring sebagai sumber alternatif bagi sebatian penunjuk. Nilai perencatan *PfGST* tertinggi telah diperolehi dengan menggunakan kulit kayu *Cinnamomum iners*, daun *Terminalia catappa*, dan daun *Phyllanthus watsonii*. Walau bagaimanapun, keputusan kinetik mencadangkan bahawa tumbuhan ini merencat *PfGST* melalui cara interaksi lain daripada bersaing dengan GSH, CDNB dan Hemin.

MOLECULAR CLONING, EXPRESSION, AND CHARACTERIZATION OF GLUTATHIONE-S-TRANSFERASE AS A NOVEL TARGET IN ANTI-MALARIAL DRUG DESIGN AND DISCOVERY

ABSTRACT

The Glutathione-S-transferases (GSTs) are group of detoxification enzymes. *Plasmodium falciparum* has a single isoform of GST (*Pf*GST) that involves in heme detoxification. While other GSTs isoforms from human (hGSTP1) and mouse (mGSTM1) are involved in apoptotic stress kinase pathway and mediate cancer cell resistance to chemotherapy. The *Pf*GST, hGSTP1 and mGSTM1 were successfully cloned and heterologously expressed in *E. coli*. Enzyme inhibition, kinetics and crystallization experiments were conducted to find potential lead compounds that inhibit *Pf*GST. The GSTs substrates, glutathione (GSH) and 1-chloro-2,4-dinitrobenzene (CDNB), as well as the known GSTs inhibitors of S-hexyl glutathione (GSX), cibacron blue (CB), ethacrynic acid (EA), hemin, protoporphyrin IX (protoIX) and 4-(2-hydroxyethyl)-1-piperazineethanesulfonic acid (HEPES) were studied. The results revealed affinities, binding modes and possible interactions between the inhibitors and *Pf*GST. Two binding sites were proposed for hemin in *Pf*GST. However, CB, GSX, EA and HEPES were unable to compete with hemin binding, thus considered unsuitable leads to dislodge hemin from its binding site. Due to its high affinity and possible interaction with hemin, the crystal structure of CB in complex with *Pf*GST was studied further using X-ray crystallography. As an alternative approach to obtain leads, molecules were computationally designed for targeting GSH binding site in *Pf*GST and destabilize hemin binding. Leads based on GSH molecule

and/or its binding pocket were searched using *de novo* approach. Three approaches were developed for reversible inhibitors using fragment-based and atom-based approaches, and one approach for irreversible inhibitors design. The isosteric-fragment replacement (IFR) and docked-fragment replacement (DFR) approaches successfully generated *de novo* ligands with free energy of binding and synthetic accessibility score were calculated for lead selection. Molecular dynamic simulation for selected IFR and DFR ligands showed that 1598-DFR maintain stable binding with free energy of binding of -16 kcal/mol and RMSD of less than 3 Å throughout simulation period of 7.5 ns. The third approach generated lead molecules by atomic assembly using Structure-Assisted Atom-based *De novo* molecular design (SAAD) which tailor made the molecular fragments to fit the binding pocket of γ -glutamyl moiety of GSH. In the last approach, irreversible specific inhibitors were designed to form covalent bond with *Pf*GST by using its unique 3-dimensional arrangement of cysteine residues. The analogues were designed to establish covalent bond with Cys101 through electrophilic moieties that replaces α -amino of the γ -glutamyl of GSH. The designed lead molecules may open a new avenue for treating malaria by reversible and irreversible inhibition of *Pf*GST. Plant extracts were screened as an alternative source for lead compounds. The highest *Pf*GST inhibition was obtained using *Cinnamomum iners* bark, *Terminalia catappa* leaves and *Phyllanthus watsonii* leaves. The kinetic results suggest that these plants inhibited *Pf*GST via competing with CDNB.

CHAPTER 1

INTRODUCTION

1.1 Problem statement

The discovery of new class of anti-malarial compounds is highly recommended specially after development of resistant strains for *Plasmodium falciparum*. The resistance is developed by mutations at enzymes or transmembranal transporters which are interacted with anti-malarial compounds. Such mutations are usually occurred close to the active site of those macromolecules and consequently disrupt their proper functions. However, the harmful biochemical consequences of such disruption can be relieved if the genome encodes other isoforms of the mutated macromolecule.

Glutathione-S-transferases (GSTs) are group of detoxification enzymes that conjugate xenobiotics or hydrophobic molecules to endogenous substrate of glutathione (GSH). The conjugation product is more polar and thus suitable for subsequent elimination from the cell (Hinchman and Ballatori, 1994). Moreover, GSTs have been reported to catalyze isomerization reactions as well as involve in small molecular carriage and protein interactions (Oakley, 2011).

The *Plasmodium falciparum* genome encodes single isoform of GST (*PfGST*) which is being involved in heme capturing (Harwaldt et al., 2002; Deponte and Becker, 2005; Hiller et al., 2006). Thus *PfGST* provides a potential target for anti-malarial drug discovery and development which could act synergistically with quinines (Harwaldt et al., 2002). The structural differences between *PfGST* and human GSTs can be involved to promote selectivity during drug design and screening (Fritz-Wolf et al., 2003).

Other GST isoforms like human Pi-1 (hGSTP1) and mouse Mu-1 (mGSTM1) have been reported to involve in apoptotic stress kinase pathway. The apoptosis signal regulating kinase-1 and its substrate C-Jun N-terminal kinase (JNK) are inactivated by interaction with mGSTM1 (Cho et al., 2001) and hGSTP1 (Adler et al., 1999), respectively. Moreover, the overexpression of hGSTP1 in malignant cells was found to promote resistance toward alkylating agents (Parker et al., 2008). Therefore, ethacrynic acid (a GST substrate and inhibitor) has been used in conjugation with chemotherapies to potentiate cytotoxicity (Tew, 1994).

Cloning of cDNAs and heterologous expression of *Pf*GST (Liebau et al., 2002), hGSTP1 (Moscow et al., 1989) and mGSTM1 (Townsend et al., 1989) have been previously conducted in *E.coli* using *Plasmodium falciparum* parasite, human lymphoblast, and mouse fibroblast as RNA sources, respectively. Biochemical and kinetic experiments have been conducted to study substrates and inhibitor binding to *Pf*GST, hGSTP1 and mGSTM1. In case of limited X-ray crystallographic data, molecular docking provides a computational aid to interpret the observed kinetic behavior for those enzymes.

Plants are considered the origin of known anti-malarial like quinine (Lee, 2002b) and artemisinin (Lee, 2002a), as well as provide diverse library for hit screening (Harvey, 2007; Guantai and Chibale, 2011). Measuring the inhibitory effect of plant extracts toward *Pf*GST, hGSTP1, and mGSTM1 has potential application for lead discovery as well as usage in malaria and cancer treatment.

Computational tools are currently being incorporated in molecular lead discovery and design. Depending on macromolecular crystal structure, high affinity molecules can be designed to fit the active site using *de novo* fragment-based or atom-based assembly. The stability and binding energy of the designed molecule at the

binding site can be tested by molecular dynamics simulation. With respect to the development of GSTs inhibitors, computational tools have seldomly being used with the exception of using combination of GRID and docking approaches to design simple GS-R derivatives (Procopio et al., 2005). Up to date, no isosteric replacements of GSH residues have been used to fully design GST inhibitors, with the exception of replacing Gly residue by tetrazole carboxylate isostere (Burg et al., 2002b) and γ -glutamyl-cysteine peptide bond with urethanic junction (Cacciatore et al., 2005). Yet, both replacements have been reported to adversely affect the activity of the prepared analogues. Several non-specific inhibitors have been developed by seeding GSH or other scaffolds (Mahajan and Atkins, 2005; Ruzza et al., 2009).

Since its discovery (Liebau et al., 2002), *Pf*GST has not been the subject for specific lead discovery and design despites being frequently reported as valuable anti-malarial target (Srivastava et al., 1999; Harwaladt et al., 2002; Fritz-Wolf et al., 2003; Deponte and Becker, 2005). Which could be an application of neglecton for a member of bottom billion problems, where support is given for financial opportunities over global health needs (Trouiller et al., 2001). Therefore, the aim of this study is to clone and heterologously express GST isoforms of *Pf*GST, hGSTP1 and mGSTM1. Enzyme kinetics and molecular docking are to be used for investigating the interaction between the GST isoforms and a group of GST inhibitors; which may shape and address potential leads. X-ray crystallography is to be used to resolve the binding mode of *Pf*GST inhibitor. Several plant extracts and fractions are to be screened for comparative inhibitory effect toward the GSTs isoforms. Computational tools are to be involved in lead molecules design and validation. Atom-based and fragment-based *de novo* molecular design approaches are to be developed and applied for *Pf*GST inhibitor design.

1.2 Malaria and anti-malarial compounds

Malaria is one of the most devastating endemically reemerging protozoal disease which is no more restricted to poor and developing countries. According to reports in 2014 from World Health Organization and Global Malaria Action Plan, malaria infects 198 million people and kills about 600,000 annually. And according to the reports, about half of world population is at risk of being infected with malaria and there are 79 malarious countries of which 20 countries are in Asia-Pacific (Figure 1.1). In spite of global spread of malaria and development of drug resistant strains, no new chemical class of anti-malarial has been introduced to clinical practice since 1996 (Gamo et al., 2010).

Malaria causative agent is the *Plasmodium* parasite. Until now, more than 100 species of *Plasmodium* have been identified (Tuteja, 2007), however at least 5 species are currently known to infect human with the most virulent being *Plasmodium falciparum* (Kantele and Jokiranta, 2011). The parasite multiplies sexually in the gut of *Anopheles* mosquito to form sporozoites which migrate to insect's saliva and is injected to host blood stream when the insect takes its meal. Subsequently, the sporozoites reach and multiply asexually in host's liver (5-15 days) before schizonts rupture and release merozoites. Merozoites infect red blood cells and occasionally form the sexually mature gametes; the forms which are suitable for multiplication in insect gut (Laurence et al., 2008).

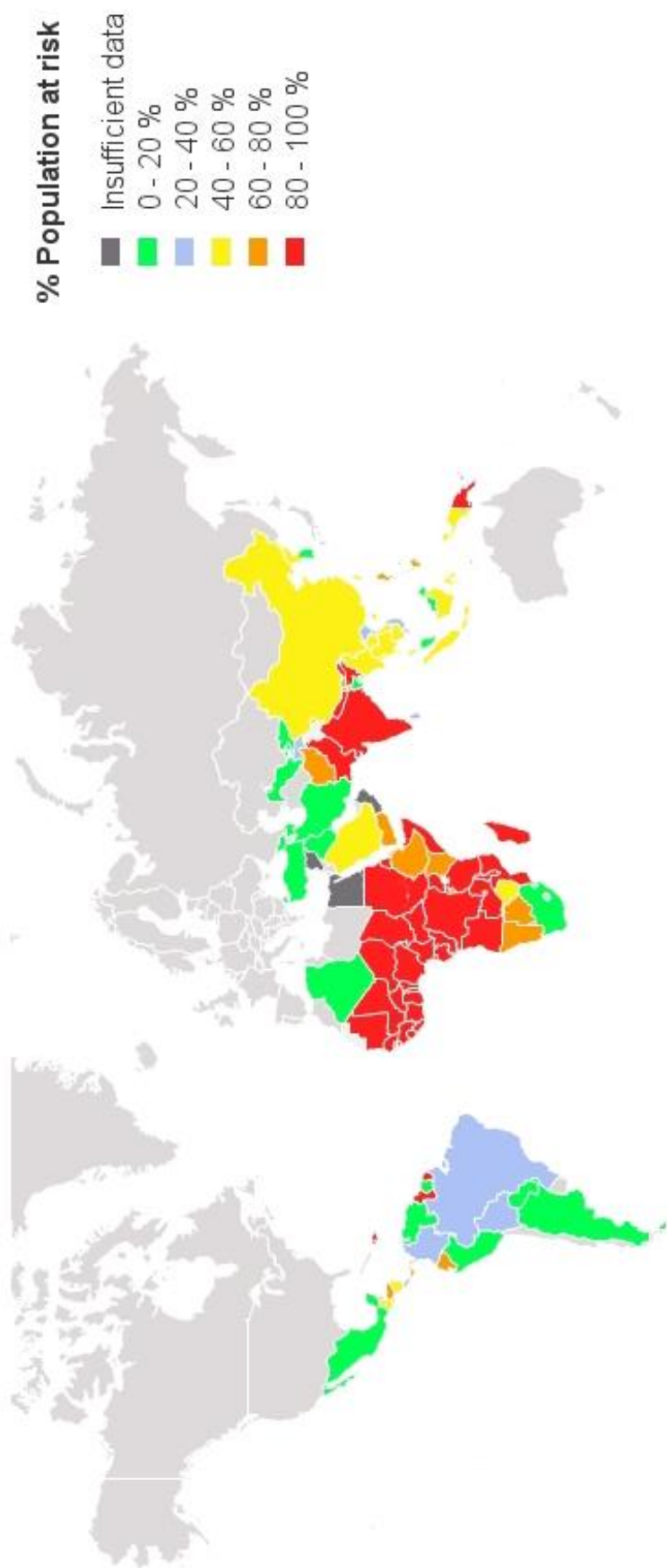


Figure 1.1: Global distribution for percentage of malaria cases caused by *Plasmodium falciparum* (WHO mapper, 2014).

During the intra-erythrocytic stage, the parasite digests cellular haemoglobin of the host to get the necessary amino acids by using several proteinases. The unavoidable consequence of haemoglobin digestion is the release of free ferroprotoporphyrin. In the presence of oxygen ferroprotoporphyrin (heme) is oxidized to ferriprotoporphyrin (hemin). This process produces superoxide, which decomposes into H_2O_2 and O_2 . The parasite detoxify free heme by crystallizing it into hemozoin (Egan et al., 2002). Anti-malarial of 4-aminoquinolines like chloroquine and amodiaquine inhibit heme accumulation into hemozoin, thus building up a toxic concentration of ferro/ferriprotoporphyrin leading to parasite death (Deharo et al., 2003).

At the host side, human body reacts against infection by production of nitrous oxide and oxygen radicals. Host reaction as well as parasitic digestion of haemoglobin and formation of free heme exaggerates the oxidative stress in the parasite. The parasite relieves the oxidative stress via glutathione and thioredoxin dependent enzymes systems (Krnajski et al., 2002; Becker et al., 2004).

Several anti-malarial compounds are available (Figure 1.2) and act at different stages through the life cycle of the parasite (Figure 1.3). Although the molecular targets have not been determined for many of the compounds, the currently known targeted pathways are mainly related to nucleic acid metabolism, heme detoxification, oxidative stress, protein digestion, fatty acid biosynthesis, and trans-membranal channels (Alam et al., 2009).

Resistance toward anti-malarial compounds is attributed to mutation in key enzymes or in compounds trans-membranal transporters. For example, resistance toward chloroquine is attributed to mutation in *Pfmdr1*, *Pfcg2* and *Pfcrt* transporters, atovaquone to mutation in cytochrome b, anti-folates (pyrimethamine and proguanil)

to mutations in dihydrofolate reductase, sulfonamides and sulfones to mutations in dihydropteroate synthase, and even artemisinin due to mutations in PfATPase6 (Olliaro, 2001; Alam et al., 2009).

The *Plasmodium falciparum* (isolate 3D7) has 23-megabase nuclear genome consists of 14 chromosomes, encodes about 5,300 genes, and is the most (A + T)-rich genome sequenced to date (Gardner et al., 2002a). Enzymes form about 15% of the predicted expressed proteins (Figure 1.4) and considered as anti-malarial targets (Table 1.1).

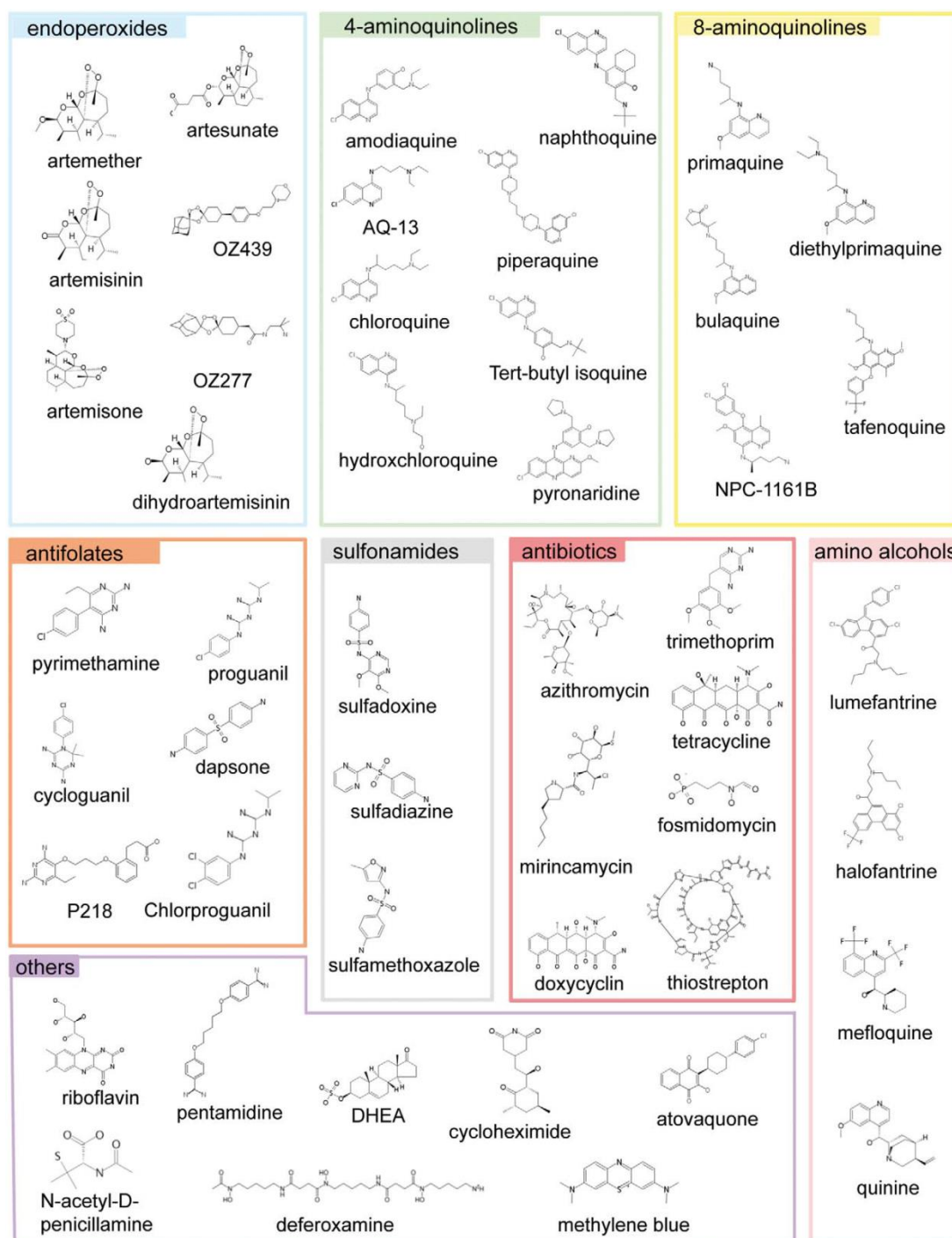


Figure 1.2: The main classes of anti-malarials. The chemical structures of all the main classes of anti-malarials and other therapeutic and control molecules are assembled according to either the chemical classes they belong to (endoperoxides, 4- and 8- AQs, amino-alcohols) or their function (antifolate, antibiotics), or both (e.g., sulfonamides, a chemical class of antibiotic used in combined anti-malarial therapies) (Delves et al., 2012).

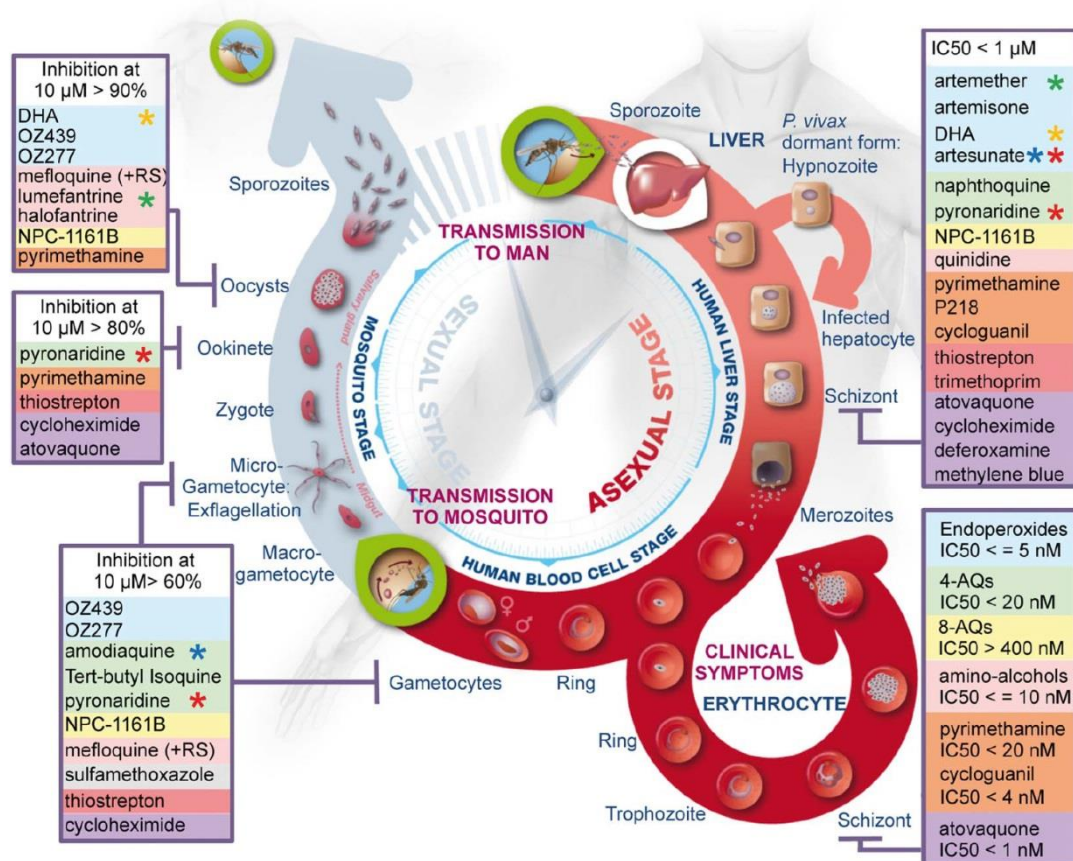


Figure 1.3: Summary of the activity of the most widely used anti-malarials throughout the life cycle of *Plasmodium*. The three main phases, i.e., liver stage, blood stage, and vector stage, of the life cycle of *Plasmodium* are shown. The two key entry points leading to transmission of the parasites from vector to host and from host to vector are indicated (green circles). Parasite forms specific to each stage are highlighted and drugs identified as inhibitors of development of these forms are listed in boxes and colored as described in previous Figure. Stars highlight components of the main artemisinin combination therapies: green, coartem; red, pyramax; orange, eurartesim; blue, ASAQ (Delves et al., 2012).

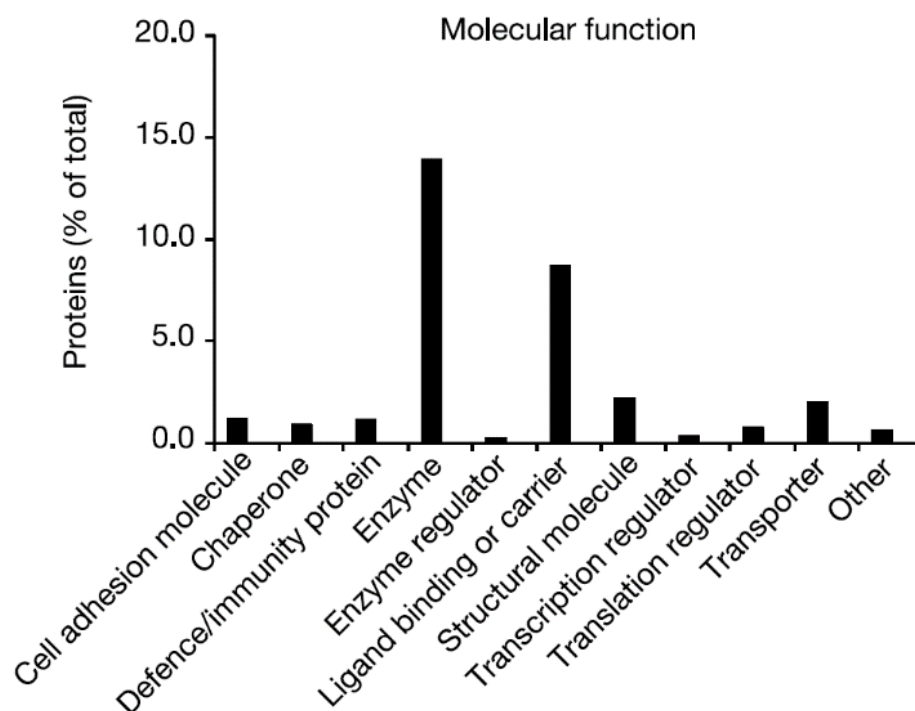


Figure 1.4: Classification of functional proteins predicted from *Plasmodium falciparum* (3D7) genome (Gardner et al., 2002a).

Table 1.1: Enzymes considered as anti-malarial targets (Mehlin, 2005; Buchholz et al., 2007; Alam et al., 2009).

Group	Enzymes
Peptidases	Plasmeprin Falcipain Aminopeptidase N falcilysin
Glycolytic enzymes	L-lactate dehydrogenase Triose phosphate Isomerase Glyceraldehyde-3-phosphate dehydrogenase Fructose-1,6-bisphosphate aldolase
Lipid metabolizing enzymes	Enoyl-acyl carrier reductase Phosphoglycerate kinase
Redox and detoxification enzymes	Glutathione reductase Thioredoxin reductase Glutathione S-transferase Glutamate dehydrogenase
Folate synthesis	Dihydrofolate reductase-thymidylate synthase
Purine salvage enzymes	Purine Nucleoside Phosphorylase Adenylosuccinate synthetase Hypoxanthine phosphoribosyltransferase

1.3 Glutathione-s-transferases (GSTs)

Glutathione-S-transferases (GSTs, E.C. 2.5.1.18) are ubiquitous family of enzymes involved preliminarily in nucleophilic substitution reactions. GSTs can bind to endogenous as well as exogenous substrates. Exogenous substrates represent drugs, industrial intermediates, pesticides, herbicides, environmental pollutants, and carcinogens. While endogenous substrates represent cell-membrane phospho-lipid hydroperoxides, oxidized products of nucleotides and catecholamines, as well as several other endogenous compounds.

GSTs were first studied as xenobiotic metabolizers before other functions were reported. Back to 1960s, the rat liver extracts showed the ability to catalyze the conjugation of 1,2-dichloro-4-nitrobenzene to glutathione tripeptide (γ -glutamyl-cysteinyl-glycine, GSH) (Figure 1.5). Other activities such as binding carcinogens, steroids and bilirubin were also reported, thus the protein was initially called 'ligandin'. The previous activities were –later on- attributed to Mu and Alpha classes of GSTs. Several classes of GSTs were discovered by using 1-chloro-2,4-dinitrobenzene (CDNB) as a more general transferase substrate as well as using bioinformatics approach (Sherratt and Hayes, 2002).

GSTs belong to phase-II detoxification enzymes that remove electrophilic compounds from the cell by conjugation to endogenous GSH. The GS-conjugates are substrates for transmembranal transporters. GSTs protect the cell from environmental and oxidative stress, xenobiotics, as well as responsible for resistance against certain drugs, therefore, have been considered a reliable target in several therapeutic designs and interventions. In this section a biological introduction will be given regarding classification, structure, functions, and medical significance of GSTs. Members of GSTs family from *Plasmodium falciparum*, human, and mouse will be considered.

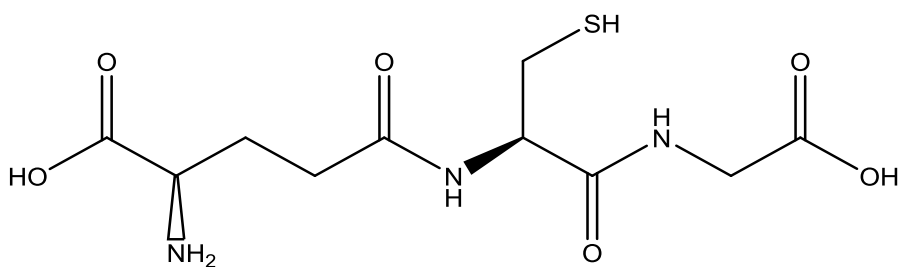


Figure 1.5: Structure of tripeptide glutathione (γ -glutamyl-cysteinyl-glycine or GSH)

1.4 Classification of GSTs

Within creatures, three classes of proteins so far have been discovered that show glutathione transferase activity. Two of them are soluble, namely cytosolic and mitochondrial GSTs. The third is membrane-bound microsomal GST also referred as membrane-associated proteins in eicosanoid and glutathione metabolism (MAPEG). Variations in structure and substrate selectivity represent the main differences between soluble and membrane-bound GSTs. Soluble forms are more directed toward drugs and xenobiotics metabolism while membrane-bound toward leukotrienes and prostaglandins metabolism. All soluble and membrane-bound GSTs can conjugate 1-chloro-2,4-dinitrobenzene to GSH and exhibit glutathione-dependent peroxidase activity toward cumene hydroperoxides (Holm et al., 2002; Hayes et al., 2005; Holm et al., 2006).

About 15-20 different cytosolic GSTs have been identified in human and mammals, 40-60 in plants, 10-15 in bacteria, and more than 10 in insects (Nebert and Vasiliou, 2004; Frova, 2006). Cytosolic GSTs can be classified into 16 classes depending on sequence similarity, immunological cross reactivity, and substrate specificity, namely: alpha, beta, delta, epsilon, zeta, theta, kappa, lambda, mu, nu, pi, sigma, tau, phi, omega and dehydroascorbate reductase (DHAR) (Mannervik and

Danielson, 1988; Salinas and Wong, 1999; Strange et al., 2000; Strange et al., 2001; Frova, 2006; Oakley, 2011). Some subclasses are ubiquitous, others are organism-specific. Currently recognized classes of cytosolic GSTs in mammals include alpha, mu, omega, pi, sigma, theta and zeta (Mannervik et al., 2005). GSTs show higher interclass sequence similarity (60-80%) than structural homology (25-35%) (Andujar-Sanchez et al., 2005)

1.5 General structure of cytosolic GSTs

Microsomal GSTs or Membrane Associated Proteins in Eicosanoid and Glutathione metabolism (MAPEGs) are present as homotrimeric membrane-spanning helical structures (Holm et al., 2006). On the other hand, soluble GSTs are all functional homo or hetero (within same class) dimeric. Each monomer is of 199–244 amino acids in length and has molecular weight from 23-28 kDa (Armstrong, 1997). It is composed of a conserved N-terminal thioredoxin domain containing GSH binding site connected to a more variable C-terminal R-helical domain containing the binding site for the GSH acceptor substrate (Hayes et al., 2005) (Figure 1.6).

The typical thioredoxin domain composed of β - α - β - α - β - α structural motif (Armstrong, 1997; Hebert and Jegerschold, 2007; Atkinson and Babbitt, 2009) (Figure 1.7). The active site within the thioredoxin domain which recognizes GSH (G site) is conserved in all classes of GSTs, however, some residues may vary among different classes. The residue of major interest in the binding site is the one which principally activates the thiol group of GSH for nucleophilic attack (Armstrong, 1997). For example, the binding site of alpha, mu, and pi classes in mammals as well as *Pf*GST utilizes tyrosine residue for GSH activation. The classes of phi and tau in plants, delta in insects as well as theta and zeta utilize serine residue. While omega in

mammals and insects, beta in bacteria, lambda and DHAR in plants utilize cysteine residue (Frova, 2006). Due to the formation of mixed disulfide bond with GSH, omega class of GSTs has poor conjugation activity, instead; it is involved mainly in redox reactions (Whitbread et al., 2005). In all of alpha, mu, and pi classes, the GSH tripeptide adopts an extended conformation running antiparallel to the conserved loop (50-53) that connects $\alpha 2$ and $\beta 3$ (Fritz-Wolf et al., 2003). The α -amino group of γ -Glu interacts with strictly conserved Gln and Asp residues. However, the fundamental interaction found in all classes of cytosolic GSTs is the hydrogen bonding between Pro residue at the N-terminus of $\beta 3$ and backbone amine of GSH cysteinyl moiety (Oakley, 2011)

The second domain contains the hydrophobic substrate binding site (H-site) and consists of a variable number (4–7) of α -helices positioned downstream the thioredoxin domain and connected to it via short loop (around 10 amino acids). GSTs sequence alignments from different species showed that about one third of the sequence differences are focalized at the H-site, thus determines the range and selectivity of chemicals metabolized by the enzyme (Armstrong, 1997). The G- and H-sites are labeled in Figure 1.11.

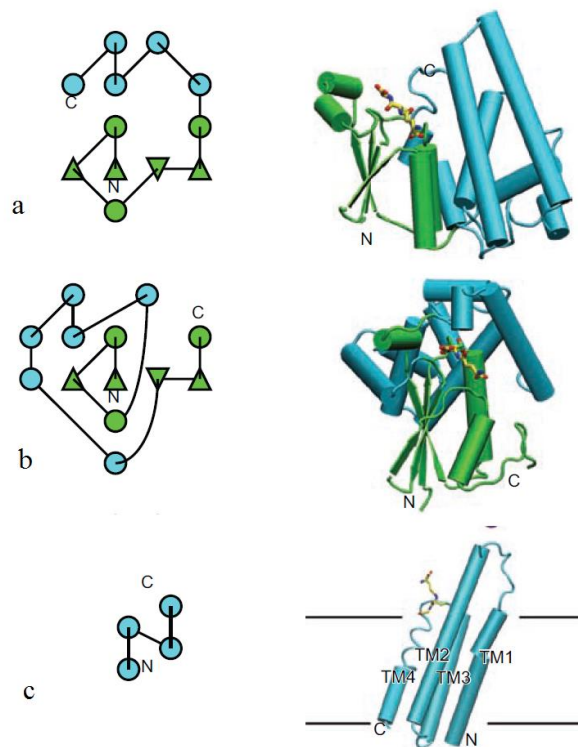


Figure 1.6: Topology and structural representations of (a) cytosolic GST, (b) mitochondrial GST, and (c) MAPEG. The thioredoxin domain (green) composed from α -helices (circles) and β -sheets (triangles). The C-terminal domain composed mainly from α -helices (Oakley, 2011).

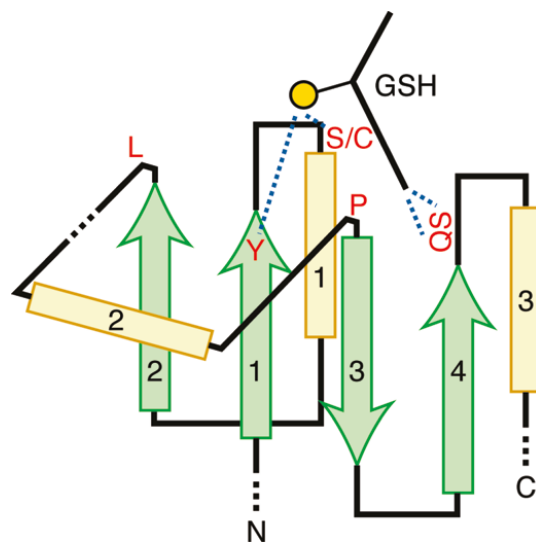


Figure 1.7: Thioredoxin domain common in soluble GSTs; it is composed from 4 beta-sheets interconnected by 3 alpha helices. The GSH binding to GST is stabilized by hydrogen bonds (dashed blue line). The GSH thiol group is activated by giving hydrogen bond to catalytic residue Tyr (Atkinson and Babbitt, 2009).

1.6 General mechanisms for catalyzing chemical reactions employed by enzymes and GSTs

Enzymes are merely catalysts for chemical reactions, they only accelerate rate of chemical reaction toward the equilibrium by lowering activation energy and not changing the equilibrium. Enzymes (E) induced strains and perturbations that convert substrate (S) to its highly energized unstable transition state structure (ES^\ddagger). The short half-life of transition state (about 10^{-13} second) is extended by binding enzymes, thus reduces the required activation energy (ΔG_{ES^\ddagger}). According to Arrhenius equation, linear lowering of activation energy separating for a given reaction, produces exponential increment in reaction rate (Equation 1.1).

$$\text{Reaction rate constant} = Ae^{-\frac{\Delta G_{ES^\ddagger}}{RT}} \quad \text{Equation 1.1}$$

Where R is the gas constant, T is the temperature in Kelvin, and A is the Arrhenius constant. Several mechanisms have been proposed for ES^\ddagger complex stabilization (Copeland, 2000):

Structural features of enzyme active site:

- Sequester the substrate from solvent effect.
- Decrease dielectric constant by the hydrophobic pocket, thus, intensifying the electric field against the substrate produced by judiciously placed charged functional groups within the active site.

Reactivity features of enzyme active site:

- Approximation of reactants and orbital steering
- Covalent catalysis (nucleophilic and electrophilic addition)

- General acid-base catalysis
- Conformational distortion
- Preorganization of the active site for transition state complementarity

GST group of enzymes catalyzes the conjugation reaction of GSH by nucleophilic addition. The enzyme active site involves in activating the thiol group of GSH to form partial covalent bond between the tyrosine or serine residue and thiolate ion of GSH. Subsequently, the activated thiolate ion can easily attack any electrophilic group of the second substrate (Graminski et al., 1989; Shan and Armstrong, 1994; Armstrong, 1997).

Generally in nucleophilic catalysis, the reaction rate depends on nucleophilic strength and electron donating ability of the attacking group which in turn directly related to basicity (pKa). Moreover, it depends on the group's oxidation potential, polarizability, ionization potential, electronegativity, potential energy of the higher occupied molecular orbital (HOMO), covalent bond strength, and general size of the group.

With respect to substrate, the reaction rate depends on the electrophilicity of the substrate functional group (i.e. how good its “leaving group” is), pKa of leaving group, hence, its state of protonation (the weaker is the base, the better is the leaving group species), and chemical nature of the leaving group (Copeland, 2000).

With respect to GSTs, the enzyme stabilizes the thiolate form of GSH, thus making it available for conjugation. All of *Pf*GST, hGSTP1, and mGSTM1 have been designed to use tyrosine residue for stabilizing GSH thiolate ion via hydrogen bond (Figure 1.8). Moreover, intra molecular interaction with the free amino group of γ -

glutamyl moiety appears to play a crucial role in activating the thiol group in GSH (Adang et al., 1988).

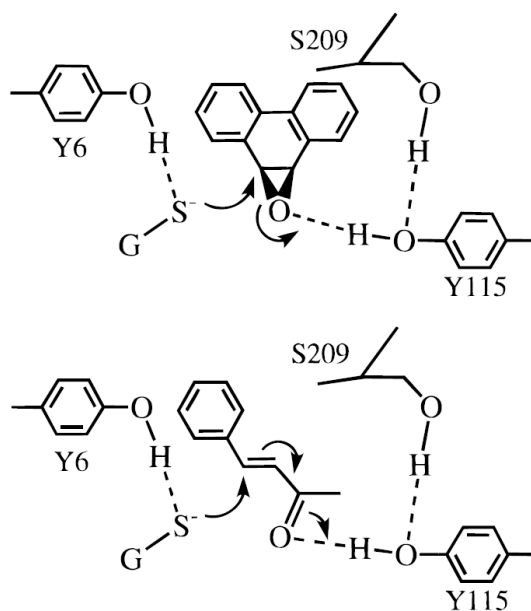


Figure 1.8: Conjugation reactions catalyzed by rate GST Mu 1-1 (rGSTM1-1, PDB 5FWG) that uses Tyr6 for activating GSH thiol group. The active thiolate group attacks a) phentrene epoxide by nucleophilic addition and b) benzylideneacetone double bond by Michaelis addition (Shan and Armstrong, 1994).

1.7 GSTs functions and substrates

The main function of GSTs is to catalyze the conjugation of GSH toward xenobiotic substrates. However, other functions are vested to GSTs including peroxide degradation, double-bond *cis-trans* isomerization, steroid and leukotriene biosynthesis, reduction and non-catalytic “ligand-in” activities.

1.7.1 Conjugation activity

GST is defined as a member of phase-II detoxification enzyme. GSTs catalyze variety of reactions involving endogenous and exogenous compounds as substrates. Nucleophilic attack of GSH to nonpolar molecules which carry electrophilic C, N, or S atoms is the most important cellular defense reaction catalyzed by GSTs. In human, GSH conjugates are, subsequently, expelled from the cell by trans-membranal ATP-Binding Cassett (ABC) transporters. GSH conjugates are then metabolized by extracellular proteins γ -glutamyltransferase and dipeptidases to sequentially remove glutamyl and glycyl moieties, respectively. Specific cells reabsorb cysteine *S*-conjugates and perform acetylation on the amino group of the cysteinyl residue by intracellular *N*-acetyl-transferases. Corresponding mercapturic acids (*N*-acetylcysteine *S*-conjugates) is then formed that can be released into the circulation and delivered to the kidney for excretion in urine, or they may undergo further metabolism (Hinchman and Ballatori, 1994)

Substrates that can be detoxified by GSTs include cancer chemotherapeutic agents specially alkylating agents such as busulfan, carmustine, chlorambucil (Parker et al., 2008), *cis*-platin, cyclophosphamide, etoposide quinone (metabolite of Etoposide), ethacrynic acid, melphalan, mitozantrone, and thiotepa. Environmental chemicals and their metabolites also detoxified by GST include acrolein, atrazine,

DDT, inorganic arsenic, lindane, malathion, methyl parathion, muconaldehyde, and tridiphan. Another important class of substrates for conjugation by GSTs is the *in vivo* products of phase-I transformation, like phenanthrene epoxide, benzo[*a*]-pyrene epoxide, and lipid peroxides (Hayes et al., 2005). Other substrates include herbicides (Marrs, 1996; Neufeind et al., 1997), pesticides, industrial intermediates, environmental pollutants, carcinogens, heterocyclic amines produced by cooking protein-rich food, arene oxides, unsaturated carbonyls, and organic halides (Hayes et al., 2005; Oakley, 2011). A list of conjugation reactions catalyzed by GSTs is provided in Figure 1.9.

1.7.2 Peroxidase activity

GSTs possess selenium-independent glutathione peroxidase activity towards organic hydroperoxides. This activity is cellular protective since it prevents organic hydroperoxides of phospholipids, fatty acids and DNA in becoming engaged in free radical propagation reactions which ultimately lead to macromolecular destruction (Hayes and Strange, 1995; Deponite and Becker, 2005). GSTs can detoxify products of lipid peroxidation (Bruns et al., 1999; Collinson et al., 2002), polycyclic aromatic hydrocarbon epoxides derived from the catalytic actions of phase 1 cytochrome P-450s as well as numerous by-products of oxidative stress (Strange et al., 2001).

1.7.3 Isomerization activity

Some GSTs isozymes are known to possess GSH-dependent isomerization activities, like isomerization of the keto steroid intermediates in testosterone and progesterone synthetic pathway (Johansson and Mannervik, 2001), the less hydrophilic maleate analogues of maleylacetoacetate (Keen and Jakoby, 1978; Fernandez-Canon and Penalva, 1998), and 13-*cis* retinoic acid (Chen and Juchau,

1998). Some GST isoforms are involved in biosynthesis of arachidonic acid derivative of eicosanoids like prostaglandins and leukotrienes (Kanaoka et al., 1997). Some parasites are able to use this characteristic of GSTs to perform GSH-dependent isomerization of some chemicals such as prostaglandins, thus modulating the host immune system during infection (Angeli et al., 2001; Ouaisi et al., 2002).

1.7.4 Toxicity potentiation activity

Opposite to detoxification, GSTs can potentiate the toxicity of some substrates by catalyzing conjugation or lysis reactions. As example GSTs increases the toxicity of some short chain alkyl halides that have two functional groups like dihalomethane, dihaloethane, isoesters, isothiocyanates, sulforaphane, and haloalkene. Moreover, GSTs can release cytotoxic drugs from prodrug contains sulfide bond such as the conversion of azathioprine to mercaptopurine (Eklund et al., 2006). This phenomenon has been efficiently incorporated in designing tumor selective chemotherapy where the overexpressed GSTs activate the release of active cytotoxic molecular fragment (Lyttle et al., 1994b; Satyam et al., 1996; Rosen et al., 2003; Ruzza and Calderan, 2013). Another example is the TER 286 which can be activated by the overexpressed GST (hGSTP1) in cancerous cells to generate nitrogen mustard alkylating agent (Morgan et al., 1998)

1.7.5 Ligand-in activity

GSTs can function as cargo proteins to carry certain organic molecules by non-productive ligand-in process (Mannervik and Danielson, 1988). Ligand-in is another mechanism to detoxify compounds under condition of lower GSH concentration (Parker et al., 2008). GSTs can carry hemin, bilirubin, bile salts, steroids (Remoue et al., 2002), thyroid hormones, fatty acids (Caccuri et al., 1990). Moreover, GSTs can

detoxify several drugs by ligand-in like adriamycin, bleomycin, mitomycin C, carboplatin (Ruzza et al., 2009), as well as the anti-inflammatory drug sulfasalazine (Oakley et al., 1999). The process of ligand-in is applied for heme transportation (Boyer and Olsen, 1991) giving hematin binding in *Haemonchus contortus* as an example of endowment for parasite to tolerate blood feeding (van Rossum et al., 2004). Moreover, it was recognized that GST in *Plasmodium falciparum* could function as a buffer for heme-containing compounds in vivo (Platel et al., 1999; Harwaldt et al., 2002; Deponte and Becker, 2005; Liebau et al., 2005).

1.7.6 Protein-interaction activity

Soluble GSTs can bind to some proteins and manipulate their functions. The protein kinases involved in apoptotic stress kinase pathway can be inactivated by interaction with some GST isoforms. The apoptosis signal regulating kinase-1 and its substrate C-Jun N-terminal kinase (JNK) are inactivated by interaction with mGSTM1 (Cho et al., 2001) and hGSTP1 (Adler et al., 1999), respectively. The oxidative or chemical stress induced by chemotherapies mediate the dissociation GST-JNK-C-Jun complex leading to apoptosis (Adler et al., 1999; Townsend, 2007).

Other functions of GSTs include reduction of dehydroascorbate and transfer of thiols (Neuefeind et al., 1997), dehydroascorbate reductase activities (Board et al., 2000), participation in cellular signaling, regulation of transcription and stress response (Salinas and Wong, 1999), as well as catalyzing formation of disulfide bonds for some hydrophobic substrates (Keen and Jakoby, 1978). Selected reactions catalyzed by GSTs are provided in Figure 1.10.

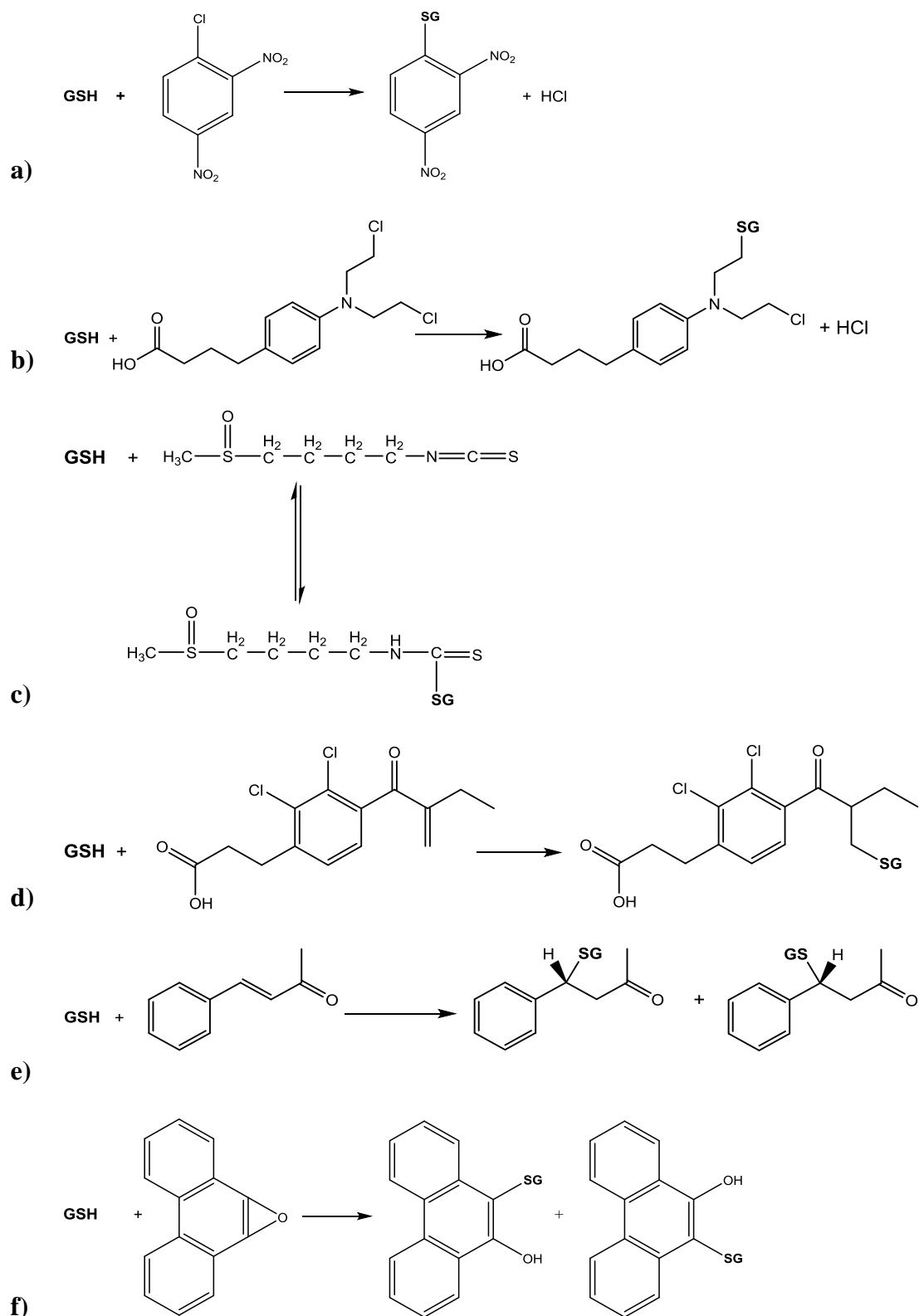


Figure 1.9: Conjugation reactions catalyzed by GST for a) 1-chloro-2,4-dinitrobenzene (CDNB), b) chlorambucil, c) sulforaphane, d) ethacrynic acid, e) benzylideneacetone, f) phenanthrene epoxide a product of cytochrome P450 catalyzed oxidation of phenanthrene.

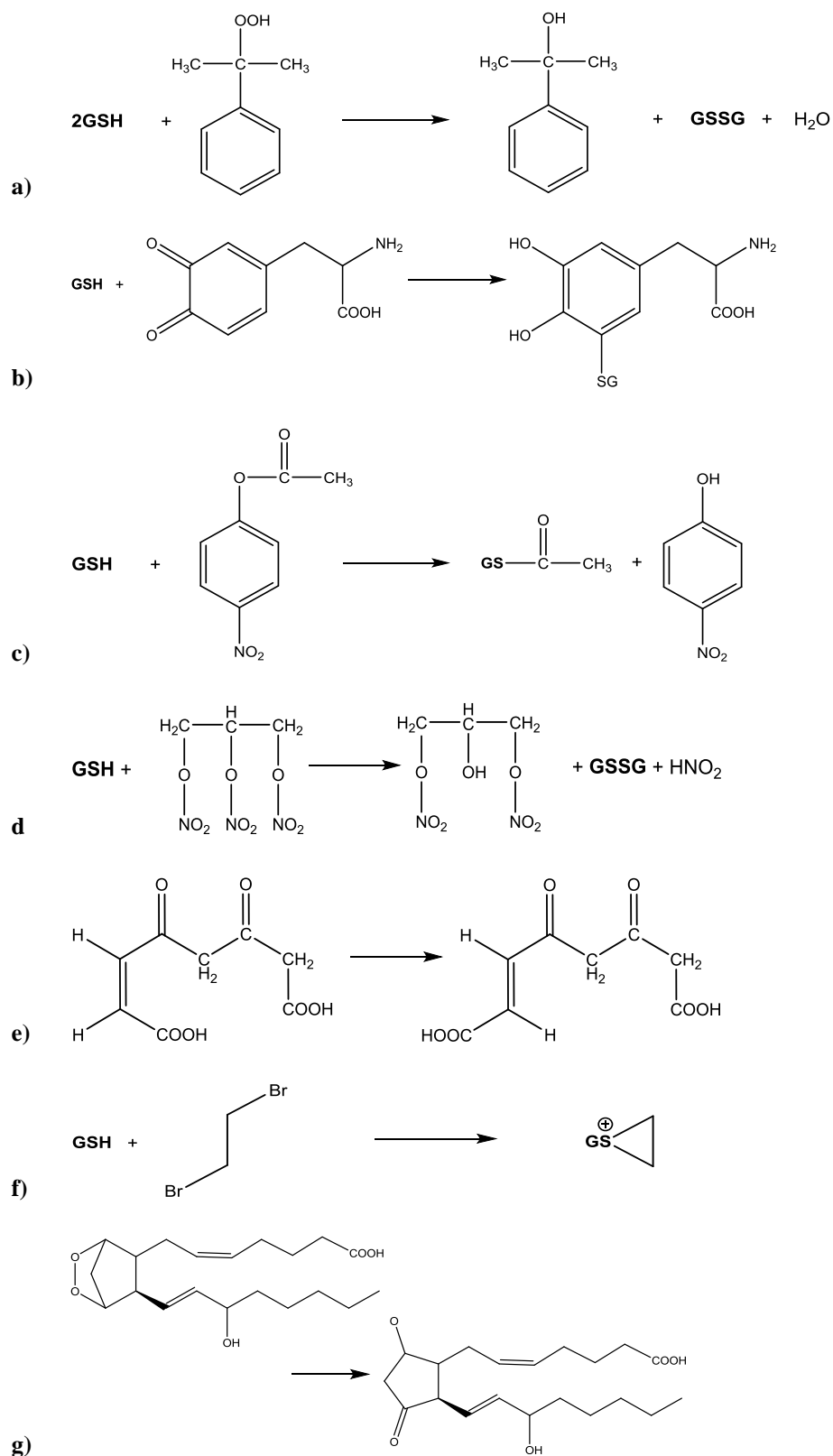


Figure 1.10: Reactions catalyzed by GST; a) reduction for cumene, b) *o*-dopaquinone conjugation, c,d) thiolysis for 4-nitrophenyl acetate and trinitroglycerin, f) isomerization of maleylacetoacetate, f) activation of 1,2-dibromoethane and g) conversion of PGH₂ to PGD₂).